Aerobic Adaptation and Metabolic Dynamics of *Propionibacterium freudenreichii* DSM 20271: Insights from Comparative Transcriptomics and Surfaceome Analysis

Iida Loivamaa[1*], Annika Sillanpää [1], Paulina Deptula[2,3], Bhawani Chamlagain[1], Minnamari Edelmann[1], Petri Auvinen[3], Tuula A. Nyman[4], Kirsi Savijoki[1,5], Vieno Piironen[1], Pekka Varmanen[1*]

[1] Department of Food and Nutrition, P. O. Box 27, University of Helsinki, FI-00014, Finland; iida.loivamaa@helsinki.fi; annika.sillanpaa@helsinki.fi; bhawani.chamlagain@helsinki.fi: minnamari.edelmann@helsinki.fi; Kirsi.savijoki@helsinki.fi; pekka.varmanen@helsinki.fi

[2] Department of Food Sciences, University of Copenhagen, 195 Frederiksberg, Denmark; deptula@food.ku.dk

[3] Institute of Biotechnology, DNA Sequencing and Genomics Laboratory, University of Helsinki, Finland; petri.auvinen@helsinki.fi

[4] Department of Immunology, University of Oslo and Oslo University Hospital, Oslo, Norway: tuula.nyman@medisin.uio.no

[5] Division of Pharmaceutical Chemistry and Technology, University of Helsinki, FI-00014, Finland; kirsi.savijoki@helsinki.fi

Running head: Transcriptomics and Surfaceomics of *Propionibacterium freudenreichii*

Address correspondence to: Iida Loivamaa, iida.loivamaa@helsinki.fi; Tel. +358-407-413-793; Pekka Varmanen pekka.varmanen@helsinki.fi; Tel. +358-29-4157057.

Abstract

Propionibacterium freudenreichii (*PFR*) DSM 20271 is a bacterium known for its ability to thrive in diverse environments and to produce vitamin B12. Despite its anaerobic preference, recent studies have elucidated its ability to prosper in the presence of oxygen, prompting a deeper exploration of its physiology under aerobic conditions. Here, we investigated the response of DSM 20271 to aerobic growth by employing comparative transcriptomic and surfaceome analyses alongside metabolite profiling. Cultivation under controlled partial pressure of oxygen (pO2) conditions revealed significant increases in biomass formation and altered metabolite production, notably of B12 vitamin, pseudovitamin-B12, propionate and acetate, under aerobic conditions. Transcriptomic analysis identified differential expression of genes involved in lactate metabolism, TCA cycle, and electron transport chain, suggesting metabolic adjustments to aerobic environments. Moreover, surfaceome analysis unveiled growth environment-dependent changes in surface protein abundance, with implications for sensing and adaptation to atmospheric conditions. Supplementation experiments with key compounds highlighted the potential for enhancing aerobic growth, emphasizing the importance of iron and α-ketoglutarate availability. Furthermore, in liquid culture, $FeSO_4$ supplementation led to increased heme production and reduced vitamin B12 production, highlighting the impact of oxygen and iron availability on the metabolic pathways. These findings deepen our understanding of *PFR*'s physiological responses to oxygen availability and offer insights for optimizing its growth in industrial applications.

Importance

The study of the response of *Propionibacterium freudenreichii* to aerobic growth is crucial for understanding how this bacterium adapts to different environments and produces essential compounds like vitamin B12. By investigating its physiological changes under aerobic conditions, we can gain insights into its metabolic adjustments and potential for enhanced growth. These findings not only deepen our understanding of *P. freudenreichii* responses to oxygen availability but also offer valuable information for optimizing its growth in industrial applications. This research sheds light on the adaptive mechanisms of this bacterium, providing a foundation for further exploration and potential applications in various fields.

Keywords: *Propionibacterium*, Actinobacteria, vitamin B12, cobalamin biosynthesis, cobamides, fermentation, aerobic, anaerobes, transcriptomics, surfaceomics,

1. Introduction

Propionibacterium freudenreichii (*PFR*) is a Gram-positive bacterium belonging to the Actinomycetota phylum. It is commonly found in dairy products, particularly Swiss-type cheeses, where it plays a crucial role in shaping the flavor compounds and texture characteristics of the cheese (1, 2). The bacterium metabolizes lactate to produce propionic acid and carbon dioxide, which leads to the formation of gas bubbles responsible for the characteristic eyes in Swiss-type cheeses (3). Besides its role in cheese production, *PFR* has garnered significant attention due to its potential health benefits, including its immunomodulatory properties and the production of vitamin B12 (hereafter B12) (2, 4, 5).

B12, also known as cobalamin, is an essential nutrient vital for various physiological processes in humans (6). Unlike many other organisms, humans cannot synthesize B12 and must obtain it from dietary sources or microbial production (7). *PFR* stands out as one of the microbial species capable of producing this essential vitamin. Its history of safe use in fermented foods and ability to produce vitamin B12 have attracted considerable interest from the food and pharmaceutical industries (8, 9). Given the prevalence of B12 deficiency, particularly among individuals following vegetarian or vegan diets, the microbial production of vitamin B12 by *PFR* offers a promising solution to address this nutritional deficiency (10).

Notably, the synthesis of cobalamin, as well as the human inactive pseudovitamin, by *PFR* exhibits intriguing dependencies on environmental conditions, particularly oxygen availability. While the first steps of cobalamin synthesis follow the anaerobic pathway where cobalt is inserted at an early stage (11), the biosynthesis of the lower ligand, 5,6-dimethylbenzimidazole (DMBI), requires oxygen. Absence of oxygen during biosynthesis leads to the production of pseudovitamin B12 (hereafter pseudo-B12) with adenine as the lower ligand (12).

PFR DSM 20271, the type strain of the species, has garnered significant attention due to its ability to produce the active form of B12 in various plant food matrices and under different applications (13-15). Furthermore, the response of DSM 20271 to oxygen and its ability to grow under aerobic conditions have attracted scientific interest. Recent studies have revealed that certain strains of *PFR*, including DSM 20271, while traditionally considered anaerobes, exhibit tolerance to oxygen. They can grow to high cell densities under mildly aerated conditions, which allow the consumption of oxygen and thereby keep levels of dissolved oxygen below the detection limit (16). The adaptation of DSM 20271 to these microaerobic conditions was shown to involve complex metabolic adjustments, affecting various cellular processes, including energy metabolism, redox

105 balance, and gene expression (16, 17). *PFR* under aerobic conditions, including detectable oxygen
106 concentrations, remains to be studied.

107 The genome sequence of DSM 20271 (18) indicates that the strain possesses enzymatic systems,
108 such as superoxide dismutase and heme-containing catalase, which likely play crucial roles in
109 protecting the bacterium against oxidative stress caused by oxygen exposure. Furthermore, like
110 other *PFR* strains (19, 20), DSM 20271 is equipped with the genes required for aerobic respiration
111 and for the complete pathway for heme synthesis. As heme iron is more easily absorbed and has a
112 higher bioavailability than other forms of iron (21), heme biosynthesis through bioprocessing of
113 food material potentially increases the nutritional value. Heme and cobalamin synthesis are
114 interconnected as both pathways begin with the formation of uroporphyrinogen III precursor (22).

115 In this study, we cultivated the DSM 20271 strain in bioreactors under control of the partial pressure
116 of oxygen (pO2), keeping it at approximately 20% by sparging with pure oxygen/air as well as under
117 anaerobic conditions by nitrogen gas sparging. Employing a comparative transcriptomic approach
118 alongside comparative surfaceome analyses and targeted metabolite profiling, we sought to
119 elucidate the bacterium's response to oxygen. The findings of this study contribute to a deeper
120 understanding of the physiological responses of *PFR* to oxygen availability and offer valuable
121 insights for optimizing its growth. Furthermore, the identification of key compounds and
122 metabolites enhancing the aerobic growth and colony-forming ability of *PFR* under aerobic
123 conditions can have significant implications for industrial applications.

124

125 **2. Results and Discussion**

126 In the present study, we used pH-controlled bioreactor cultivations to investigate the cellular
127 responses of DSM 20271 during growth under aerobic and anaerobic conditions. Our focus was on
128 monitoring the central growth characteristics, the production of B12 and pseudo-B12 vitamins, and
129 the major metabolic end products **(Fig. 1A)** at specific time points of growth and conditions **(Fig.**
130 **1B)**. These findings were complemented with transcriptomic analyses and validated with label-free
131 quantitative proteomics on cell surface proteins at the indicated timepoints **(Fig. 1B)**. Additional
132 follow-up studies were conducted to confirm the most relevant metabolic processes.

133

134

135

136

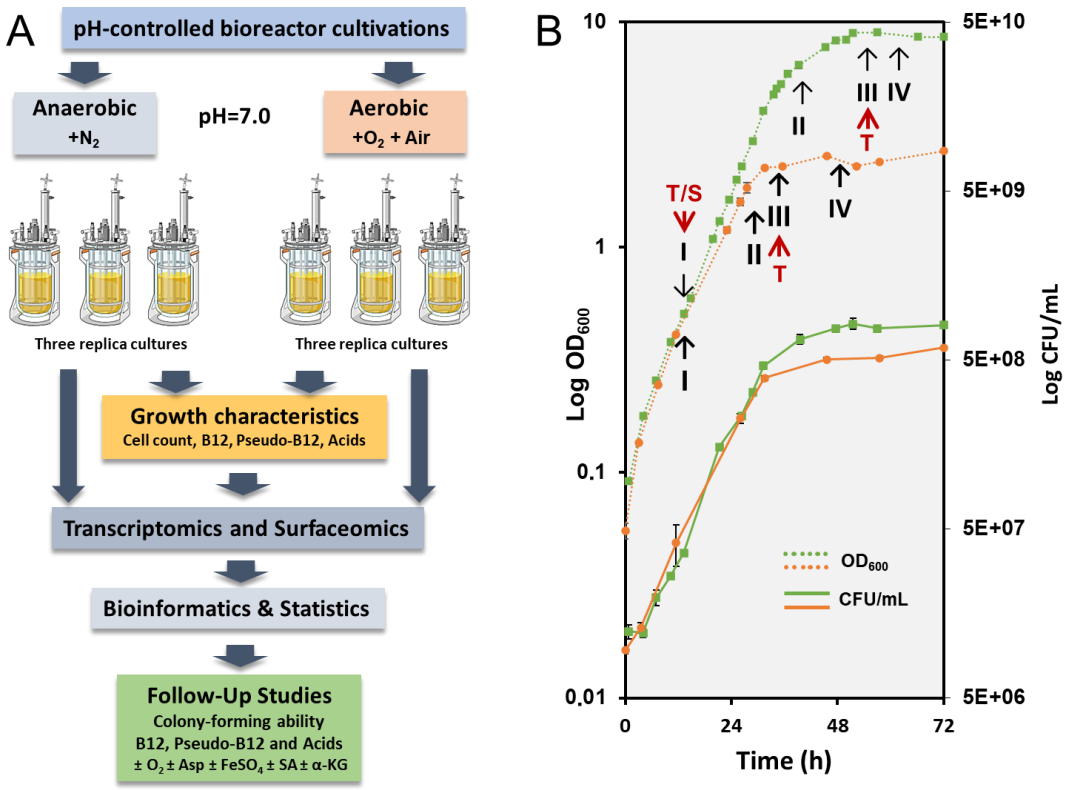

Figure 1. (**A**) A workflow illustrating an overview of experiments including bioreactor cultivations and parameters studied as well as follow-up growth experiments conducted in supplemented media. Asp, aspartate; SA, succinate; α-KG, α-ketoglutarate. **(B)** Cell densities (dotted line) and cell viability (solid line) in bioreactor-conducted experiments under aerobic (green) and anaerobic (orange) growth conditions. Sampling points for OD_{600} measurement and determining colony-forming units are marked with circles (anaerobic) and squares (aerobic). For the analysis of key metabolite production dynamics and transcriptomics over time, samples were taken at four growth stages: mid-logarithmic (I), late logarithmic (II), early stationary (III), and late stationary (IV) phases. RNA sequencing was performed on samples I and III. Arrows in red indicate the timepoint/growth stage of *PFR* at which the cells were withdrawn for transcriptomics (T) and surfaceomics (S).

2.1 Oxygen affects lactate metabolism, biomass, and formation of organic acids, B12, and pseudo-B12

Formation of biomass. To initiate the characterization of the response of DSM 20271 to aerobic growth, the strain was cultivated in bioreactors at a constant pO2 level of 20% and compared the growth characteristics to control cultivation under anaerobic control conditions (pO2 level below the detection limit). A pO2 level of 20% was selected based on preliminary experiments indicating that higher oxygen concentrations no longer increased cell density (Loivamaa et al., unpublished data). A significant increase in biomass formation was observed under aerobic conditions with a pO2 level of 20% compared to anaerobic conditions. Specifically, the cell densities determined at 600 nm and viable cell counts on agar (CFU/mL) were 3.2 and 1.4 times higher, respectively, under the maintained aerobic atmosphere over the 72-hour-cultivation **(Fig. 1B)**.

159 ***Secretion of organic acids.*** Lactate was found to be consumed faster under anaerobic conditions
160 but was depleted from the media under both conditions in the early stationary phase sample (III)
161 **(Fig. 2A)**. Under anaerobic conditions, the levels of propionate and acetate in the growth medium
162 increased over time, especially during logarithmic growth **(Fig. 2B and 2C)**. In contrast, under
163 aerobic conditions, only low levels of propionate were detected in logarithmic phase samples, with

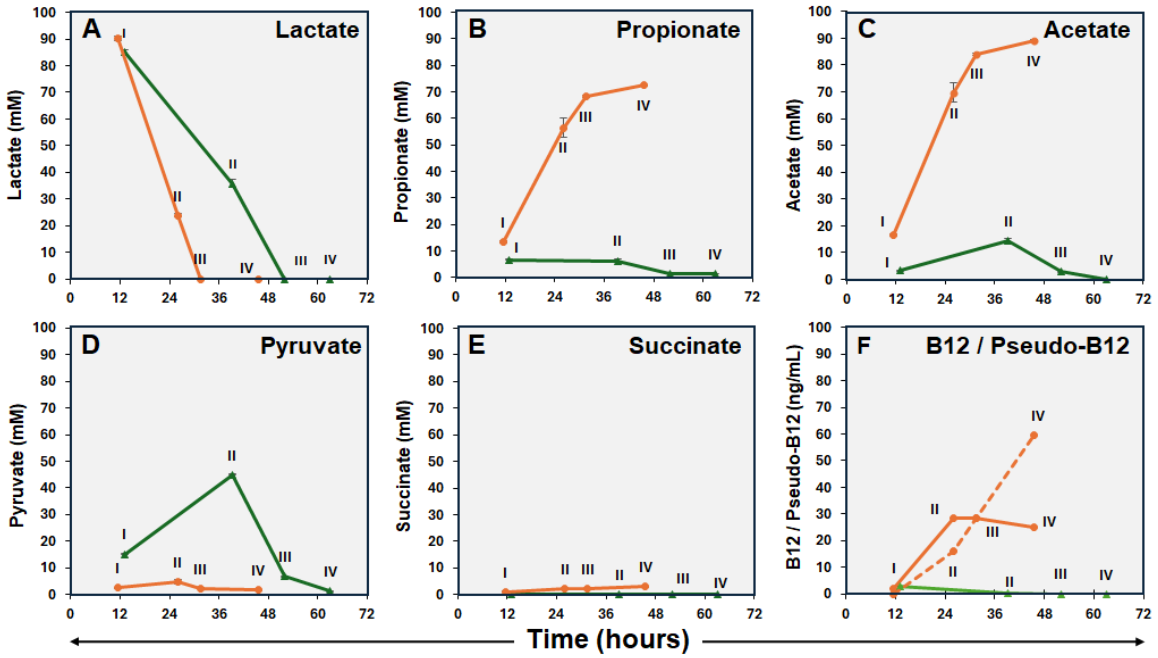

164 **Figure 2.** Lactate utilization (A), excreted propionate (B), acetate (C), pyruvate (D), succinate (E) and
165 intracellular vitamin B12 and pseudovitamin (F; vitamin B12 - solid line, pseudovitamin – dashed line) of PFR
166 DSM 20271 during cultivation under aerobic (green) and anaerobic (orange) fermentations performed in
167 bioreactors. N = 3, except pseudovitamin samples III and IV: n=2. No pseudovitamin was detected under
168 aerobic growth conditions.

169

170 levels dropping below the limit of detection in stationary phase samples. Acetate levels followed a
171 similar pattern under aerobic conditions, being fully depleted from the medium after an initial
172 increase **(Fig. 2C)**. During logarithmic growth, the pyruvate levels in the media were higher under
173 aerobic conditions but decreased to low levels in stationary phase samples **(Fig. 2D)**, whereas
174 succinate was only detected in growth media in samples from anaerobic conditions **(Fig. 2E)**.
175 Pyruvate in culture supernatants, at concentrations reflecting its intracellular levels in *PFR*, has been
176 reported previously (23), but to the best of our knowledge, there are no reports of the effect of
177 atmospheric conditions. As the elevated growth under aerobic conditions is accompanied by
178 diminished lactate consumption and, on the other hand, increased pyruvate excretion, it is
179 tempting to assume that ATP production is maintained by upregulation of the later stages of the

180 aerobic respiration pathway. The accumulation of succinate during adaptation to anaerobic or
181 oxygen-limiting conditions has been previously observed in *Mycobacterium tuberculosis* (24).

182 ***Synthesis of B12 and pseudo-B12***. B12 and pseudo-B12 levels were analyzed in cellular and
183 supernatant (media) samples. However, no B12 or pseudo-B12 was detected in the media of either
184 aerobic or anaerobic cultivations. Under aerobic conditions, the concentration of B12 in the cells
185 was very low at each sampling point and below the detection limit at sampling points II-IV **(Fig. 2F)**.
186 Under anaerobic conditions, B12 reached 28.5 ng/mL as fermentation progressed, while the
187 concentration of pseudo-B12 increased as the fermentation process approached completion and
188 reached 59.8 ng/mL. **(Fig, 2F)**. It is noteworthy that cultivation of this strain in our bioreactors under
189 identical conditions but with no gas sparging, thus resembling microaerobic conditions, resulted in
190 superior B12 production. The levels were 1.7 to 4.9 times higher compared to anaerobic conditions,
191 along with a distinct metabolite production pattern **(Fig. S1)**.

192 In a previous study (16), the DSM 20271 strain was cultivated in bioreactors under conditions with
193 an oxygen supply at a level that allowed its concentration to drop below the detection limit in the
194 culture through consumption by cellular activity. Like those microaerobic conditions, aerobic
195 conditions used here were found to increase biomass production compared to anaerobic
196 conditions. However, the metabolite production profile under aerobic conditions seems to differ
197 from those reported under microaerobic conditions. Firstly, lower oxygen concentrations promoted
198 propionate production during the lactate consumption phase followed by its oxidation to acetate
199 (16) **(Fig. S1)**. Under the more aerobic conditions used here, the consumption of lactate from the
200 media was not accompanied by propionate accumulation. Furthermore, the B12 production
201 appears to be drastically affected by increasing oxygen concentration, as microaerobic conditions
202 increased B12 production compared to anaerobic conditions (17) **(Fig. S1)**, which is opposite to
203 what was observed here under aerobic conditions **(Fig. 2F)**. The ratio of B12 to pseudovitamin in
204 microaerobic conditions was not analyzed in previous studies due to the use of a microbiological
205 assay that does not distinguish between them (17). Here, we observed that the active form of B12
206 is produced under microaerobic conditions, whereas very low levels of either B12 or pseudo-b12
207 are produced under aerobic conditions **(Fig. 1; Fig. S1).** Thus, the typical features associated with
208 *PFR* as an efficient producer of B12 and short-chain fatty acids, such as propionate and acetate, do
209 not apply under aerobic growth conditions.
210

211 **2.2 Transcriptomics of DSM 20271 under anaerobic and aerobic conditions**

212 In this study, we used gene expression data to uncover genes important for growth in both aerobic
213 and anaerobic atmospheres, with focus on genes contributing to the growth of *PFR* under aerobic
214 conditions as neither the physiology of this species in aerobic environments nor gene expression
215 has yet been extensively studied (16). The gene expression of strain DSM 20271 grown under
216 aerobic and anaerobic conditions was compared by isolating the total RNA from cells at the mid-
217 logarithmic (sampling point I) and stationary phases (sampling point III) of growth for RNA
218 sequencing.

219 To specifically identify differences between growth phases and conditions, pairwise differential
220 expression analyses were utilized. A total of 1376 genes were found to be differentially expressed
221 at sampling point I, with an adjusted p-value (padj) of < 0.05. Among these, 713 genes were
222 downregulated, and 663 genes were upregulated under aerobic conditions. Additionally, 906 genes
223 showed differential expressions at sampling point III. Out of the 906 genes, 388 genes were
224 downregulated, and 518 genes were upregulated under aerobic conditions **(Fig. 3)**. A list of
225 differentially expressed genes, annotation results, and expression levels of under anaerobic and
226 aerobic atmospheres at sampling points I and III are shown in **Table S1**.

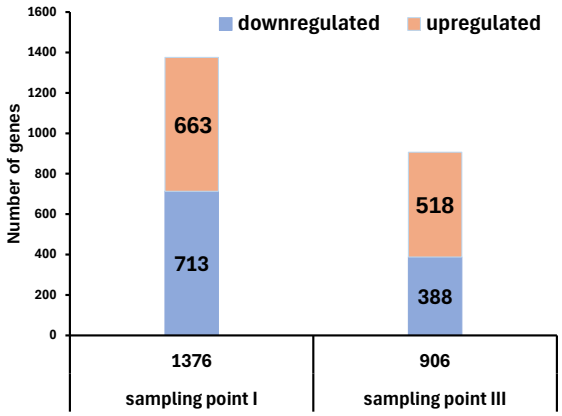

227 **Figure 3.** The number of genes exhibiting differential expression in *PFR* DSM 20271 cultivated under aerobic compared
228 to anaerobic atmospheres. Pairwise analyses of differential expression were conducted to identify variances between
229 growth environments. During sampling point I, 1376 genes showed significant differential expression (adjusted p-value
230 < 0.05), with 713 genes downregulated and 663 genes upregulated. Similarly, at sampling point III, 906 genes displayed
231 differential expression, with 388 genes downregulated and 518 genes upregulated.

232 ***Gene ontology (GO) enrichments.*** GO enrichments were conducted to obtain a comprehensive
233 understanding of the functional groups represented by the differentially expressed genes (DEGs).
234 The putative functions of the DEGs were further classified into various categories using the gene
235 ontology (GO) framework. At sampling point I, the DEGs were organized into nine distinct GO
236 categories, exhibiting statistical significance ($p < 0.05$). This categorization involved a comparison

237 between the aerobic and anaerobic growth conditions. These categories encompassed
238 transmembrane transport, transmembrane transporter activity, ATPase activity, zinc ion binding,
239 magnesium ion binding, 4 iron, 4 sulfur cluster binding, 'de novo' IMP biosynthetic process,
240 transferase activity, transferring glycosyl groups, and carbohydrate metabolic process **(Fig. 4A)**.
241 Similarly, at sampling point III, the DEGs were categorized into 11 GO categories, with statistical
242 significance observed ($p < 0.05$). These categories included structural constituent of ribosome,
243 translation, rRNA binding, ribosome, plasma membrane, tRNA binding, glycolytic process, DNA
244 recombination, peptidoglycan biosynthetic process, cytoplasm, and transferase activity;
245 transferring acyl groups **(Fig. 4B**).

246 ***Lactate metabolism.*** Analyses of organic acids from bioreactor cultivations revealed that lactate
247 consumption was more rapid under anaerobic conditions compared to the aerobic atmosphere
248 (Figure 2 A). The gene RM25_RS08745 encodes L-lactate permease and is the first gene within a
249 predicted four-gene operon (RM25_RS08730–RM25_RS08745). This operon also contains genes
250 encoding lactate utilization proteins A, B, and C. These proteins exhibit homology to the *lldEFG*-
251 encoded proteins found in *Shewanella oneidensis* (25) in which together with lactate
252 dehydrogenase (LDH), they form an enzyme complex responsible for catalyzing the oxidation of
253 both D- and L-lactate stereoisomers to pyruvate (25). In our study, the expression levels of these
254 operon genes were upregulated under anaerobic conditions in both sampling points (I and III).
255 Specifically, in the III samples, the fold difference in expression ranged from 2.4 to 3.9, which
256 correlates with the observed lactate consumption results. Regardless of the atmospheric
257 conditions, the lactate utilization operon was downregulated upon shifting to the stationary phase.

258 The DSM20271 strain possesses two paralogs of LDH, namely RM25_RS04460 and RM25_RS05095,
259 which encode NAD-dependent L-lactate dehydrogenases. Additionally, it carries one FAD-
260 dependent D-lactate dehydrogenase encoded by RM25_RS01945. Under anaerobic conditions in
261 the later sampling points (III), the expression level of D-lactate dehydrogenase was found to be 3.8-
262 fold higher compared to aerobic conditions. These findings suggest that lactate metabolism is more
263 active when oxygen is limited (anaerobic conditions). Multiple pathways are available for the
264 conversion of pyruvate into acetyl-CoA. Two enzymes, the pyruvate dehydrogenase complex and
265 pyruvate ferredoxin oxidoreductase, can perform this conversion. In this study, the gene cluster
266 encoding pyruvate dehydrogenase (*pdh*), specifically genes RM25_RS01015, RM25_RS01020, and
267 RM25_RS01025, showed significantly higher expression levels (2.0-8.6-fold) under aerobic
268 conditions (at both sampling points, I and III). On the other hand, one of the two paralogs encoding
269 pyruvate ferredoxin oxidoreductase, RM25_RS00920, only displayed higher expression (2.8-fold)

under anaerobic conditions in later samples. These findings indicate that different pathways for pyruvate conversion are utilized under aerobic and anaerobic conditions.

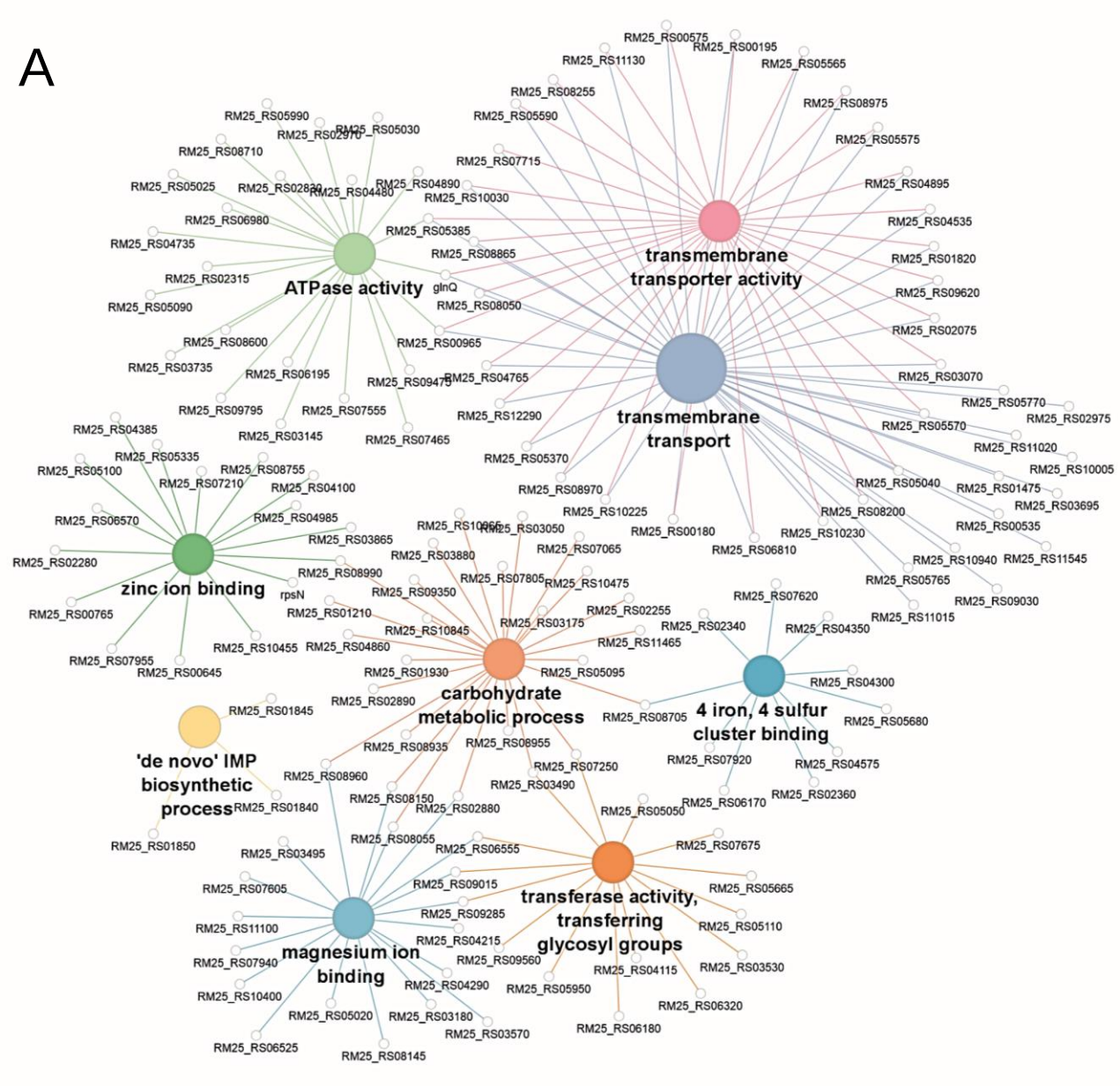

Figure 4. Gene Ontology (GO) classification of differentially expressed genes (DEGs) at sampling point I **(A)** and sampling point III **(B)** was conducted. At sampling point I, DEGs' putative functions were categorized into nine distinct GO categories, all exhibiting statistical significance ($p < 0.05$). At sampling point III, DEGs were distributed across 11 distinct GO categories with statistical significance ($p < 0.05$). The size of the spheres corresponds to the number of genes within each gene ontology category. A straight line emerging from each sphere, representing a category, is connected to a gene. A single gene may be associated with multiple categories, depicted as multiple connections from one gene to several spheres.

280

B

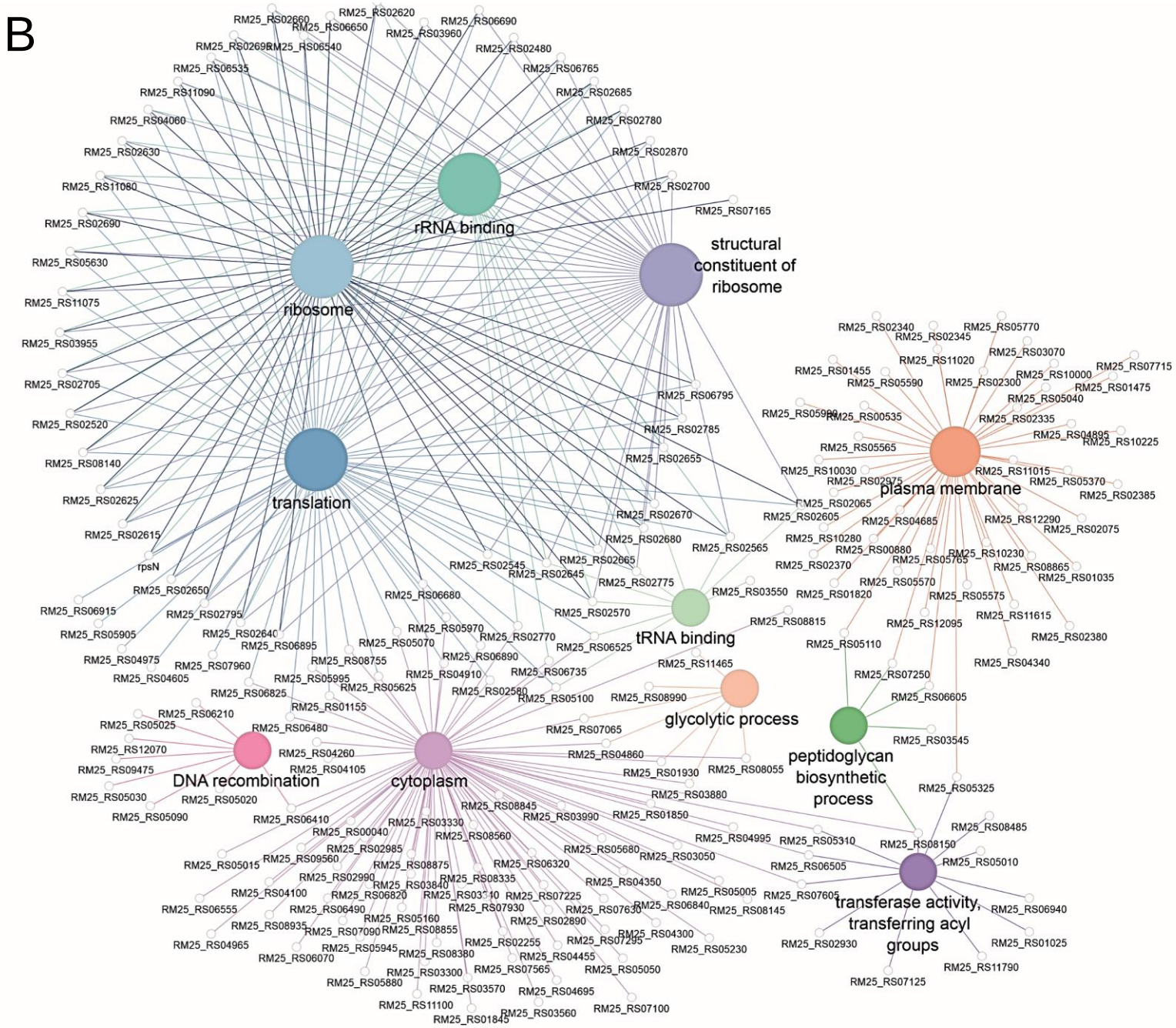
rRNA binding
structural constituent of ribosome
ribosome
translation
plasma membrane
tRNA binding
glycolytic process
peptidoglycan biosynthetic process
DNA recombination
cytoplasm
transferase activity, transferring acyl groups
RM25_RS02660
RM25_RS02620
RM25_RS06650
RM25_RS06690
RM25_RS03960
RM25_RS0269
RM25_RS06540
RM25_RS02480
RM25_RS06535
RM25_RS06765
RM25_RS11090
RM25_RS02685
RM25_RS04060
RM25_RS02780
RM25_RS02630
RM25_RS02870
RM25_RS11080
RM25_RS02700
RM25_RS07165
RM25_RS02690
RM25_RS05630
RM25_RS11075
RM25_RS03955
RM25_RS02705
RM25_RS06795
RM25_RS02520
RM25_RS02785
RM25_RS08140
RM25_RS02655
RM25_RS02625
RM25_RS02615
RM25_RS02670
RM25_RS02680
RM25_RS02565
rpsN
RM25_RS02545
RM25_RS02645
RM25_RS02665
RM25_RS02650
RM25_RS02775
RM25_RS06680
RM25_RS03550
RM25_RS06915
RM25_RS02795
RM25_RS02570
RM25_RS05905
RM25_RS02640
RM25_RS05970
RM25_RS02770
RM25_RS06895
RM25_RS05070
RM25_RS06525
RM25_RS04975
RM25_RS07960
RM25_RS08755
RM25_RS06890
RM25_RS04605
RM25_RS05995
RM25_RS04910
RM25_RS06735
RM25_RS05625
RM25_RS02580
RM25_RS06825
RM25_RS05100
RM25_RS08990
RM25_RS01155
RM25_RS06210
RM25_RS05025
RM25_RS06480
RM25_RS07065
RM25_RS12070
RM25_RS04260
RM25_RS04860
RM25_RS09475
RM25_RS04105
RM25_RS01930
RM25_RS08055
RM25_RS05030
RM25_RS05020
RM25_RS03880
RM25_RS05090
RM25_RS08845
RM25_RS06410
RM25_RS03330
RM25_RS03990
RM25_RS01850
RM25_RS00040
RM25_RS08560
RM25_RS02985
RM25_RS05680
RM25_RS04995
RM25_RS05310
RM25_RS09560
RM25_RS03050
RM25_RS05015
RM25_RS08875
RM25_RS06320
RM25_RS06505
RM25_RS02990
RM25_RS08335
RM25_RS04350
RM25_RS03840
RM25_RS04100
RM25_RS06820
RM25_RS03310
RM25_RS07225
RM25_RS05005
RM25_RS07605
RM25_RS06555
RM25_RS06490
RM25_RS07930
RM25_RS07630
RM25_RS06840
RM25_RS08145
RM25_RS05160
RM25_RS02890
RM25_RS08935
RM25_RS07090
RM25_RS08855
RM25_RS04300
RM25_RS04965
RM25_RS05945
RM25_RS02255
RM25_RS07295
RM25_RS05230
RM25_RS06070
RM25_RS08380
RM25_RS04455
RM25_RS03300
RM25_RS07565
RM25_RS05050
RM25_RS05880
RM25_RS03570
RM25_RS04695
RM25_RS11100
RM25_RS03560
RM25_RS07100
RM25_RS01845
RM25_RS02340
RM25_RS05770
RM25_RS02345
RM25_RS03070
RM25_RS11020
RM25_RS07715
RM25_RS01455
RM25_RS10000
RM25_RS05590
RM25_RS02300
RM25_RS01475
RM25_RS05040
RM25_RS05590
RM25_RS00535
RM25_RS02335
RM25_RS04895
RM25_RS10225
RM25_RS05565
RM25_RS10030
RM25_RS11015
RM25_RS02975
RM25_RS05370
RM25_RS02385
RM25_RS02065
RM25_RS02605
RM25_RS04685
RM25_RS12290
RM25_RS02075
RM25_RS10280
RM25_RS00880
RM25_RS10230
RM25_RS02370
RM25_RS05765
RM25_RS08865
RM25_RS01035
RM25_RS05570
RM25_RS01820
RM25_RS05575
RM25_RS11615
RM25_RS08815
RM25_RS12095
RM25_RS02380
RM25_RS05110
RM25_RS04340
RM25_RS11465
RM25_RS07250
RM25_RS06605
RM25_RS03545
RM25_RS05325
RM25_RS08485
RM25_RS08150
RM25_RS05010
RM25_RS06940
RM25_RS02930
RM25_RS01025
RM25_RS11790
RM25_RS07125

281 ***Propionate metabolism.*** The gene cluster RM25_RS08835 to RM25_RS08850 encodes the key
282 enzyme, methylmalonyl-CoA carboxytransferase (MMC), of the propionate-forming Wood-
283 Werkman cycle. Interestingly, this gene cluster was found to be constitutively expressed under the
284 conditions investigated in this study. This finding is consistent with a previous study by
285 Brzuszkiewicz et al. (26), which also observed constitutive expression of the MMC genes at both
286 logarithmic and stationary growth phases in closely related bacterium *Cutibacterium acnes*.
287 Additionally, it aligns with the study conducted by Dank et al. (16), where proteins involved in the
288 Wood-Werkman cycle were found to be as abundant in propionate consumption as in lactate
289 consumption phases in *PFR*. The TCA cycle utilizes acetyl-CoA and converts NAD+ to NADH as part
290 of its metabolic reactions. Certain genes encoding enzymes involved in the TCA cycle, such as citrate
291 synthase (RM25_RS11475), α-ketoglutarate decarboxylase (RM25_RS05675), and isocitrate
292 dehydrogenase (RM25_RS03180), exhibited higher expression levels under aerobic conditions in
293 sampling point III. These results indicate that aerobic conditions promote increased expression of
294 these TCA cycle enzymes, which contribute to the utilization of acetyl-CoA and the generation of
295 NADH. The fermentation of pyruvate by propionibacteria typically produces propionic and acetic
296 acids, as well as significant amounts of other products, such as succinate (27).

297 ***Expression of succinate dehydrogenase and other respiratory complexes.*** The primary function of
298 the succinate dehydrogenase (Sdh) complex in bacteria is to catalyze the oxidation of succinate to
299 fumarate while transferring electrons to the electron transport chain. The genome of DSM20271
300 harbors two gene clusters encoding the subunits of the Sdh complexes. These clusters consist of
301 three genes each, namely RM25_RS06150, RM25_RS06155, RM25_RS06160, and RM25_RS06655,
302 RM25_RS06660, RM25_RS06665. Here, the *sdh* gene clusters exhibited distinct patterns of gene
303 expression under different atmospheric conditions. Specifically, the cluster RM25_RS06150 to
304 RM25_RS06160 demonstrated a significantly higher expression level (2.8-3.4-fold increase) during
305 anaerobic conditions (I and III samples). Conversely, at sampling point III, the RM25_RS06655 and
306 RM25_RS06660 genes of the other cluster exhibited significantly higher expression levels (2.3 and
307 2.8-fold increase) under aerobic conditions. Based on the different expression patterns observed,
308 we propose that the gene cluster RM25_RS06655 to RM25_RS06665 is responsible for encoding
309 Sdh, catalyzing the conversion of succinate to fumarate, and is involved in both the TCA cycle and
310 aerobic respiration. In contrast, the gene cluster RM25_RS06150 to RM25_RS06160 is responsible
311 for encoding fumarate reductase, which reduces fumarate to succinate during anaerobic
312 respiration. This is also consistent with the accumulation of succinate in the medium under
313 anaerobic conditions and its absence from the medium under aerobic conditions. These two sets of

314 succinate dehydrogenase/fumarate reductase complexes have been reported earlier in various
315 studies on *Propionibacterium* strains (16, 19, 28), providing further support to our findings.
316 Furthermore, it has been suggested, but not yet explored, that in *Acidipropionibacterium*
317 *acidipropionici* the other succinate dehydrogenase complex could function in anaerobic
318 fermentation as fumarate reductase, and another complex in aerobic fermentation as succinate
319 dehydrogenase (28).

320 Expression of the NADH dehydrogenase complex, encoded by the gene cluster RM25_RS02335 to
321 RM25_RS02400, and the expression of the cytochrome-bd oxidase, encoded by genes
322 RM25_RS00880 to RM25_RS12185, were not significantly influenced by atmospheric conditions.
323 However, the gene cluster RM25_RS05560 to RM25_RS05595, which encodes the ATP synthase
324 enzyme complex, demonstrated higher expression levels under aerobic conditions, particularly in
325 the later sampling point (III). This indicates that ATP synthesis is more efficient in the presence of
326 oxygen which correlates with the results that ATP yields have been higher under aerobic growth
327 conditions (Loivamaa et al., unpublished data). These findings align with the conducted study by
328 Dank et al. (16), where they observed that the respiratory pathway remains consistently active
329 under both anaerobic and microaerobic conditions.

330 The expression of the NADH dehydrogenase complex, the cytochrome-bd oxidase, and the ATP
331 synthase complex were found to be impacted differently by the growth phase. The gene cluster of
332 the NADH dehydrogenase complex (RM25_RS02335 to RM25_RS02400) and the ATP synthase
333 enzyme complex (RM25_RS05560 to RM25_RS05595) showed downregulation at the onset of the
334 stationary phase. In contrast, the cluster of cytochrome-bd oxidase (RM25_RS00880 to
335 RM25_RS12185) was either constitutively expressed under both atmospheric conditions and, in the
336 case of RM25_RS00880, exhibited a 2.5-fold increase in expression at the stationary phase under
337 anaerobic conditions.

338 ***Synthesis of B12 and heme.*** B12 and heme are tetrapyrrols that play crucial roles in various
339 biological processes. Vitamin B12 serves as an essential coenzyme for enzymatic reactions,
340 particularly in the metabolic pathways involved in amino acid and nucleotide synthesis (29). Heme,
341 however, is involved in important cellular oxidative metabolic pathways, such as oxygen
342 transportation, response to oxidative stress, and oxidative phosphorylation. In our study, we
343 observed a significant effect of atmospheric conditions on cobalamin production by DSM20271 in
344 bioreactor cultivations. The cobalamin biosynthesis genes in *PFR* are mainly located in three
345 clusters: RM25_RS02055 to RM25_RS02075, RM25_RS03590 to RM25_RS03625, and
346 RM25_RS04745 to RM25_RS04770. Cluster RM25_RS02055 to RM25_RS02075 forms the locus for

347 cobalt transport, while RM25_RS03590 to RM25_RS03625 and RM25_RS04745 to RM25_RS04770
348 encode the assembly and activation of the corrin ring (19, 30).

349 Additionally, there are single genes, such as RM25_RS02940 (*bluB-cobT2*), RM25_RS03660 (*cobQ2*),
350 and RM25_RS05545 (*cobA*), involved in cobalamin biosynthesis. Under aerobic conditions during
351 later sampling point (III), the genes RM25_RS02070 (*cbiN*) and RM25_RS02075 (*cbiM*) encoding
352 cobalt transport proteins showed significant upregulation (4.7- and 3.2-fold, respectively), while the
353 expression of all the other B12 biosynthetic genes was not significantly affected by the atmospheric
354 conditions. The regulatory mechanism of the B12 biosynthetic pathway is known to involve
355 cobalamin riboswitches, which were predicted as located upstream of RM25_RS03590 (*cbiL*),
356 RM25_RS04770 (*cobD*) and RM25_RS02075 (*cbiM*) (31, 32). Cobalamin riboswitch controls gene
357 expression through transcriptional and/or translational modifications (33, 34). Notably, the
358 function of riboswitch upstream of *cbiM* was recently characterized in *PFR* strain P.UF1, which
359 revealed control at the transcriptional level (31). Our results are in line with this and indicated
360 significantly differential transcription of the *cbiM* and *cbiN* genes under the conditions used. On the
361 other hand, differential B12 production and the constitutive expression of other B12 genes under
362 studied conditions suggest regulation by means other than at the transcriptional level.

363 5-Aminolevulinic acid (ALA) is a precursor metabolite involved in the biosynthesis of tetrapyrrole
364 compounds, which in *PFR* is synthesized via the C5 pathway (35-37). In this pathway, ALA is
365 synthesized from glutamate through the coordinated actions of glutamyl-tRNA synthetase
366 (encoded by *gltX*), glutamyl-tRNA reductase (encoded by *hemA*), and glutamate semialdehyde
367 aminotransferase (HemL). HemB converts two ALA molecules into porphobilinogen (PBG), which is
368 further polymerized into hydroxymethylbilane (HMB) by HemC. This HMB is then transformed into
369 uroporphyrinogen III, a crucial intermediate in heme and B12 synthesis, by uroporphyrinogen III
370 synthase. Our study identified significant upregulation (2.2–3.2-fold) of ALA and uroporphyrinogen
371 III synthesis genes, specifically *hemA* (RM25_RS08900), *hemB* (RM25_RS08870), and *hemL2*
372 (RM25_RS09040), under aerobic conditions during later sampling point (III). However, the
373 expression of genes involved in later steps of heme biosynthesis, such as RM25_RS09440 encoding
374 putative uroporphyrinogen III synthase, *hemH* (RM25_RS08875), *hemY* (RM25_RS08880), and
375 *hemE* (RM25_RS12355), did not show significant differential expression in response to atmospheric
376 conditions. Furthermore, the expression of RM25_RS09440 was found to be affected by the growth
377 stage and downregulated during the shift to the stationary phase under both atmospheric
378 conditions.

379 ***Transport of iron and α-ketoglutarate are increased under aerobic conditions.*** The results of the
380 GO enrichment analysis revealed a significant impact on "transmembrane transport." To delve
381 deeper into this observation, genes from DSM 20271 were filtered based on annotations related to
382 "transport," "import," or "export," resulting in 208 genes potentially encoding transport functions.
383 Within this pool of 208 genes, nine demonstrated more than a two-fold upregulation under aerobic
384 conditions at sampling point I, and 24 exhibited more than a two-fold upregulation under aerobic
385 conditions at sampling point III **(Table 1)**. Conversely, among these 208 genes, 74 displayed more
386 than a two-fold upregulation under anaerobic conditions compared to aerobic conditions at
387 sampling point I. Subsequently, at the later sampling point (III), 34 genes were observed to be
388 upregulated under anaerobic conditions **(Table S2)**.

389 Among the transport genes that exhibited upregulation during aerobic conditioning at sampling
390 point I; three genes (RM25_RS09245, RM25_RS09250, and RM25_RS01195) are predicted to be
391 involved in either iron uptake systems or siderophore-mediated iron uptake systems. Iron plays a
392 vital role as an essential component of electron transport chains and respiratory enzymes, such as
393 cytochromes, as well as in the functioning of catalase and peroxidases, which protect reactive
394 oxygen species (ROS). Additionally, the gene *glpT* (RM25_RS01240), encoding the glycerol-3-
395 phosphate transporter, was upregulated by 2.6- and 4.1-fold under aerobic conditions at sampling
396 points I and III, respectively. Furthermore, the gene RM25_RS04570, encoding the α-ketoglutarate
397 permease, was upregulated under aerobic conditions. This permease facilitates the transport of α-
398 ketoglutarate across the cell membrane, ensuring its availability for utilization in the TCA cycle,
399 enabling subsequent energy production through oxidative phosphorylation. Four other predicted
400 transport genes that were upregulated under aerobic conditions at sampling point I, are associated
401 with the transportation of different molecules, including cations (RM25_RS02225), lipoproteins
402 (RM25_RS07080), myo-inositol (RM25_RS08970), and ions (RM25_RS12135).

403 ***Fe-S cluster biogenesis is upregulated in response to aerobic conditions.*** The SUF (Sulfur
404 mobilization) system is a crucial mechanism involved in the biogenesis of iron-sulfur (FeS) clusters,
405 which play a critical role in aerobic growth by mobilizing and utilizing sulfur. The SUF system is
406 responsible for assembling iron-sulfur clusters, which serve as vital cofactors in the proper
407 functioning of numerous enzymes and proteins (38, 39). Notably, in *Mycobacterium tuberculosis*,
408 the SUF system is the sole machinery responsible for the biogenesis of Fe-S clusters (40). In the
409 DSM2071 strain, the SUF system is likely encoded by a gene cluster consisting of eight genes, namely
410 RM25_RS06965 to RM25_RS07000. Among these genes, the last gene in the cluster
411 (RM25_RS07000, sufR) is likely responsible for encoding the transcriptional regulator, while the

412 function of the first gene (RM25_RS06965) remains unknown. Interestingly, the expression levels
413 of the genes within this cluster are upregulated by 4.7-8.3-fold under aerobic conditions, specifically
414 at sampling point III.

415 ***Transfer of amino groups from aspartate/alanine to α-ketoglutarate is upregulated under aerobic***
416 ***conditions.*** While the majority of the amino acid metabolism-associated genes showed increased
417 expression under anaerobic conditions **(Table S1)**, RM25_RS06515 coding for a putative alanine or
418 aspartate transferase was over 2 times more expressed under aerobic in comparison to the same
419 gene under anaerobic conditions at both sampling points. This indicates that this pathway, involved
420 in the production of pyruvate and glutamate or oxaloacetate and glutamate, is more active during
421 aerobic growth.

422 **Table 1.** List of transport-, import-, or export-associated genes expressed more than 2-fold in DSM 20271 at sampling
423 point I (nine genes) and sampling point III (24 genes) under aerobic conditions compared to anaerobic conditions.
424

Locus tag	Protein name	Fold-change[a]
Sampling point I		
RM25_RS07080	ABC transporter, ATP-binding protein	**5.02**
RM25_RS01195	Putative iron-siderophore transport system, periplasmic binding protein	**3.67**
RM25_RS02225	Putative cation-transporting P-type ATPase	**3.45**
RM25_RS09250	Ferrous iron transport protein A	**2.70**
RM25_RS12135	MscS transporter, small conductance mechanosensitive ion channel	**2.67**
RM25_RS01240	Glycerol-3-phosphate transporter	**2.60**
RM25_RS04570	Alpha-ketoglutarate transporter, MFS super	**2.23**
RM25_RS09245	Ferrous iron transport protein B	**2.18**
RM25_RS08970	MFS transporter, sugar porter family protein	**2.16**
Sampling point III		
RM25_RS02070	Cobalt transport protein CbiN	**4.66**
RM25_RS09620	D-serine/D-alanine/glycine transporter	**4.27**
RM25_RS01240	Glycerol-3-phosphate transporter	**4.14**
RM25_RS09250	Ferrous iron transport protein A	**4.07**
RM25_RS05305	Putative sulfonate/nitrate/taurine transport system substrate-binding	**3.92**
RM25_RS03735	ATP-binding cassette protein, ChvD family	**3.57**
RM25_RS07080	ABC transporter, ATP-binding protein	**3.22**
RM25_RS02075	Cobalt transport protein CbiM	**3.21**
RM25_RS02225	Putative cation-transporting P-type ATPase	**3.17**
RM25_RS08710	ATP binding protein of ABC transporter for sugars	**2.88**
RM25_RS03575	LAO/AO transport system ATPase	**2.72**
RM25_RS08050	Putative cationic amino acid transport integral membrane protein roce	**2.62**
RM25_RS02025	Low affinity inorganic phosphate transporter membrane protein pitA	**2.61**
RM25_RS05380	High-affinity branched-chain amino acid transport ATP-binding protein livG	**2.53**
RM25_RS05770	ABC-type dipeptide transport system, periplasmic componen	**2.49**
RM25_RS04530	Trk family potassium (K+) transporter, NAD+ binding protein	**2.46**
RM25_RS01470	Methionine import ATP-binding protein MetN 2	**2.3**
RM25_RS01195	Putative iron-siderophore transport system, periplasmic binding protein	**2.29**
RM25_RS01475	ABC D-methionine transporter, permease component	**2.26**
RM25_RS11530	ABC transporter domain-containing permease component	**2.19**
RM25_RS00345	ABC-2 type transport system integral membrane protein	**2.16**
RM25_RS10625	Putative potassium transport system protein kup	**2.09**
RM25_RS00035	ABC-type antimicrobial peptide transport system	**2.02**
RM25_RS00535	Putative polar amino acid ABC transporter substrate-binding protein	**2.01**

425 ***a)*** *The fold-changes were calculated by exponentiating the log2Fold values, which were derived from the differential*
426 *expression analysis performed using DESeq2.*

427 **2.3 The surfaceome of PFR is influenced by the atmosphere**

428 As proteins exposed at the cell surface (surfaceome) of a bacterium play multiple roles in sensing,
429 responding, and adapting to changing atmospheric conditions, we next complemented the
430 transcriptome data with proteomics. To this end, we conducted an additional bioreactor cultivation
431 analysis with DSM 20271, harvested the cells at the mid-logarithmic growth phase under both the
432 anaerobic and aerobic conditions, and subjected the washed cells in triplicate to surfaceome
433 shaving with trypsin and label-free quantitative (LFQ) proteomics.

434 ***Peptidoglycan-degrading enzymes were detected as most abundant on PFR cell surfaces.*** A total
435 of 965 proteins were identified in the present study and these proteins along with their predicted
436 subcellular locations and motifs are listed in **Table S3.** Eight proteins were exclusively identified in
437 aerobic conditions, while 19 were exclusively identified in anaerobic conditions **(Fig. 5A, Table S4)**.
438 Among these proteins, 938 were found in cells cultivated under both environmental conditions
439 **(Figure 5A)**, with 85 proteins harboring a signal peptide (Sec/SPI, Sec/SPII, or Tat/SPI type) and 79
440 proteins with 2–14 transmembrane domains, directing the protein outside of the cells or into the
441 cell membrane, respectively. Cytoplasmic proteins comprised the largest group (n, 634), suggesting
442 that the proteins might have entered the cell surface in yet unknown fashion **(Fig. 5B)**.

443

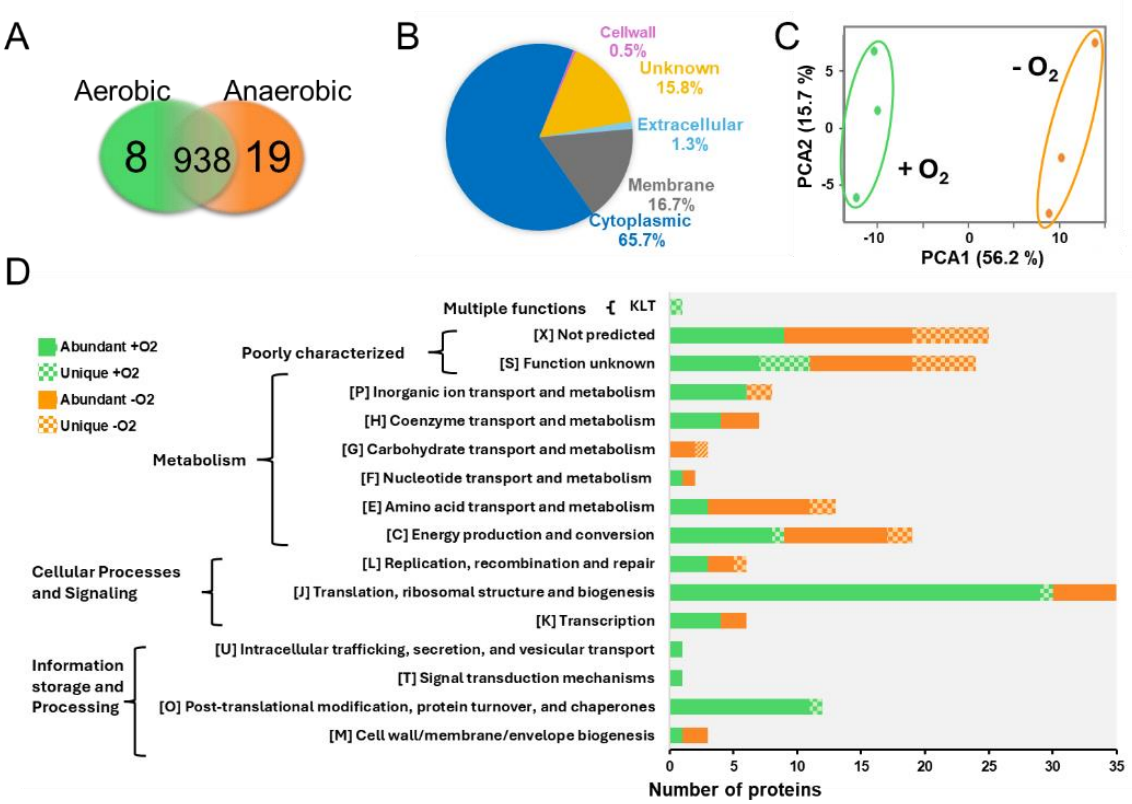

Figure 5. **Proteomic analysis of *PFR* DSM 20271T surfaceomes**. **(A)** The Venn diagram indicates uniquely and intersectively identified proteins in aerobic and anaerobic growth environments. **(B)** Subcellular localization of the identified surfaceomes (predicted by EggNOG 5.0.0). **(C)** The principal component analysis (PCA) plot of the LFQ intensities of the individual samples with 3 replicates. PCA identifies a correlation between the protein abundance profiles between aerobically (green) and anaerobically (orange) cultured bacterial cells. **D)** Functional categorization of proteins that were either uniquely identified from aerobic (green) or anaerobic (orange) culture or differentially abundant between the two growth environments (predicted by EggNOG 5.0.0).

Proteins identified with the highest intensity values, all of which have also been identified in previous studies from the cell surface or the extracellular milieu of *PFR* (Table 2) (4, 41) are likely to represent the most abundant surface proteins in DSM20271, five were found to be differentially abundant in response to atmospheric conditions after the LFQ analyses.

Locus tag	Protein name	MW (kDa)	PsortB[a]	TMDs[b]	LipoP[a]	SignalP[a]	Anaerobic			Aerobic		
							1	2	3	1	2	3
RM25_RS11635	Large surface protein A -LytG	137.3	EC	0	SPI	SP(Sec/SPI)						
RM25_RS02195	**Cell-wall peptidases, NlpC/P60 family**	**58.8**	**EC**	**0**	**SPI**	**SP(Sec/SPI)**						
RM25_RS00630	**Secreted peptidoglycan-binding RpfA**	**20.0**	**EC**	**0**	**SPI**	**SP(Sec/SPI)**						
RM25_RS02805	Resuscitation-promoting factor -RpfB	37.7	EC	1	SPI	SP(Sec/SPI)						
RM25_RS03900	DSBA-like thioredoxin domain protein	28.4	NN	1	SPI	OTHER						
RM25_RS08655	**60 kDa chaperonin 1 -GroL1_2**	**56.5**	**C**	**0**	**CYT**	**OTHER**						
RM25_RS11160	Bifunctional penicillin-binding PonA1	75.5	M	1	CYT	OTHER						
RM25_RS02990	**60 kDa chaperonin 1 -GroL1_1**	**56.1**	**C**	**0**	**CYT**	**OTHER**						
RM25_RS02580	**Translation elongation factor - EfTU**	**43.7**	**C**	**0**	**CYT**	**OTHER**						
RM25_RS12825	Hypothetical protein	113.9	CW	1	SPI	SP(Sec/SPI)						

Table 2. Top ten proteins identified with the highest raw intensity values (average of three independent replica samples). Color code, low (blue) and high (orange) protein abundances. Proteins in bold show statistically significant abundance change between the indicated conditions.
a) *PSORTb v.3.0.3, and the presence of possible classical and non-classical signal peptide sequences were analyzed with LipoP 1.0 and SignalP 5.0.* ***b)*** *The number of transmembrane spanning domains (TMD) was predicted using TMHMM 2.0, subcellular localization of proteins was done with prediction tool.*

GroL1_1, GroL1_2, and RpfA were more abundant under aerobic conditions, whereas Ef-Tu and the NlpC/P60 family-secreted peptidase were more abundant during anaerobic growth. NlpC/P60 peptidases are a family of peptidoglycan hydrolases involved in bacterial cell wall turnover and division, as well as interaction with the environment (42). GroL and Ef-Tu belong to typical cytosolic moonlighting proteins, which exhibit a second function on the cell surface of various bacteria (43). The reported moonlighting surface functions of Ef-Tu include mediating attachment to human intestinal cells and mucins (44) and functioning as an environmental sensor (45). A large number of different biological moonlighting functions have been ascribed to chaperonin 60 (Hsp60) proteins (46). Notably, a recent study revealed antiadipogenic activity of surface-exposed Hsp60 in *P.*

473 *freudenreichii* strain MJ2 (47). For *Helicobacter pylori* Hsp60, extracellular properties include iron
474 binding (48), an ability that could be beneficial in aerobic conditions, thus explaining differential
475 surface abundance in response to atmospheric conditions for *PFR*. However, the moonlighting
476 functions of Ef-Tu and the two GroL proteins of *PFR* remain still to be studied. RpfA belongs to
477 resuscitation-promoting factors that in *M. tuberculosis* have been shown to mediate resuscitation
478 from dormancy via a mechanism involving peptidoglycan hydrolysis (49). The increased abundance
479 of both RpfA and LytG with a predicted glucosaminidase domain suggests their potential roles in
480 controlling the autolysis of the *PFR* cells.

481 ***Ribosomal moonlighters were more abundant within the aerobic-surfaceomes.*** The principal
482 component analysis (PCA) of the LFQ intensities of each detected cell surface protein was applied
483 to explore the statistically significant differences ($p < 0.05$) in protein abundances between the
484 anaerobic and aerobic growth conditions. The PCA plot in **Fig. 5C** explains over 70% of the total
485 variation with a clear clustering for each aerobic and anaerobic-associated surfaceome. Both
486 surfaceomes demonstrate a strong negative (aerobic) and positive (anaerobic) correlation,
487 respectively, indicating that *PFR* responded to oxygen level alterations by introducing specific
488 protein abundance changes at the cell surface. These oxygen-dependent changes result from either
489 gene expression alterations or changes in protein secretion and/or stability.

490 An additional two-sample t-test (FDR 0.05) showed that the LFQ intensities of 139 proteins were
491 significantly differentially abundant on the cell surface between the two growth conditions **(Table**
492 **S5)**. Among these, 88 proteins were more abundant in aerobically cultivated cells, while 51 proteins
493 were more abundant in anaerobically cultivated *PFR* cells. The largest proportion of distinct or
494 differentially abundant surface proteins mainly fell under the functional category of translation,
495 ribosomal structure, and biogenesis **(Fig. 5D)**. This aligns with a previous report that the largest
496 number of intracellular/surface moonlighting protein candidates identified in various bacterial
497 surface proteomics studies belong to this functional category (50). Most of the proteins were
498 ribosomal proteins (r-proteins) from both the small (Rps) and large (Rpl) ribosomal subunits, which
499 are commonly associated with the cellular process of translation in the cytoplasm. Ribosomal
500 proteins have been identified in surfaceome studies of various bacterial species (50-54). Here, the
501 r-proteins were more abundant on the aerobic surfaceome compared to these proteins detected
502 on anaerobic cell surfaces. While we did not observe significantly increased transcription of genes
503 encoding r-proteins in log phase samples, the differential surface abundance is not likely the result
504 of differential gene expression. A Similar finding has been demonstrated in *Lacticaseibacillus*

505 *rhamnosus* GG, in which a ribosomal protein L2 (RPL2) bile-dependent abundance change occurred
506 (53).

507 Interestingly, the majority of the differentially abundant ribosomal proteins identified here have
508 previously been identified from the vesicles produced by *PFR* (5, 55, 56). In these studies, the
509 proteins delivered by vesicles contributed to translation, ribosomal structure, and biogenesis.
510 Proteomics data obtained from membrane vesicles of two *Limosilactobacillus reuterii* strains
511 identified over 50 ribosome-associated proteins (57) and similar findings have been reported for *S.*
512 *aureus, Bacillus anthracis*, *and Streptococcus pneumoniae* (58-60). These observations suggest that
513 vesicles may serve as a means for transporting ribosomal proteins to the external surroundings and
514 neighboring cells. Rodovalho et al., (5) also proposed that in response to environmental stress, *PFR*
515 might exhibit an enhanced ability to produce vesicles. In *L. reuterii* DSM 17938 strain the oxygen
516 stress influenced both the number of membrane vesicles and the protein concentration of *L.*
517 *reuteri*-derived membrane vesicles (57). Consequently, further investigation is warranted to
518 understand how the oxidative stress response affects the morphological, biochemical, and
519 biological characteristics of *PFR*-secreted vesicles.

520 Taken together, the surfaceome data suggest that the release of cytoplasmic proteins depends on
521 growth conditions rather than trypsin-triggered cell lysis, as several of these proteins were uniquely
522 detected in one condition only, while expressed under both conditions. This is in line with many
523 other studies reporting the presence of cytoplasmic proteins on the cell surface of various bacteria,
524 and it is proposed that their controlled release or export involves phages, autolysins, hydrolytic
525 enzymes, and/or vesicles (61-67). Thus, the increased abundance of RpfA and LytG on aerobic cell
526 surfaces could be one of the factors explaining the oxygen-dependent increase in the abundance of
527 r-proteins at the PFR cell surface. Additionally, changes in externally provided oxygen might have
528 affected the physicochemical characteristics of the cell surface in such a way as to stimulate the
529 binding of certain cytoplasmic proteins, as bacteria are known to modify their cell surface
530 hydrophobicity and charge in response to environmental changes (68). Since r-proteins are typically
531 negatively charged and their gene expression did not show significant atmospheric-dependent
532 changes, the externally provided oxygen could have altered the negative net charge of the bacterial
533 cell surface, as observed in some bacteria (69, 70). Therefore, aerobic conditions could have
534 promoted the binding of these proteins to the cell surface, either directly or indirectly through
535 oxygen-triggered gene expression changes affecting the charge and hydrophobicity of the cell
536 surface.

537

538 **2.4 Increasing availability of key compounds and metabolites can enhance aerobic growth of PFR**

539 Omics data suggest that pathways involving iron and α-ketoglutarate transport and metabolism, as
540 well as succinate metabolism, are more active under aerobic conditions. This data also suggest that
541 alanine/aspartate transferase activity is necessary when *PFR* is exposed to oxygen. Aspartate
542 aminotransferase catalyzes the transamination of aspartate and α-ketoglutarate, forming
543 glutamate and oxaloacetate, both of which are intermediate metabolites in the TCA cycle, alongside
544 α-ketoglutarate and succinate. Thus, it could be that increased availability of iron, aspartate, α-
545 ketoglutarate, or succinate influences the aerobic growth of *PFR*. To test this, the colony formation
546 of DSM 20271 together with another *PFR* type strain (DSM4902) on YEL agar with and without
547 FeSO4, aspartate, α-ketoglutarate, or succinate both under aerobic and anaerobic conditions were
548 compared **(Fig. 6)**. Earlier studies reported an inability of *PFR* to form colonies under aerobic
549 conditions (71, 72), whereas a recent study demonstrated that DSM 20271 thrives in the presence
550 of oxygen (16), implying strain-dependent differences in cells response to oxygen. Our results
551 revealed that under anaerobic conditions, 4 days after incubation at 30 °C, colonies were formed
552 equally by both strains. However, after 6 days of incubation under aerobic conditions, no visible
553 separate colonies of DSM4902 formed without supplementation, whereas miniscule colonies of
554 DSM 20271 were observed **(Fig. 6)**. Notably, addition of FeSO4 and α-ketoglutarate significantly

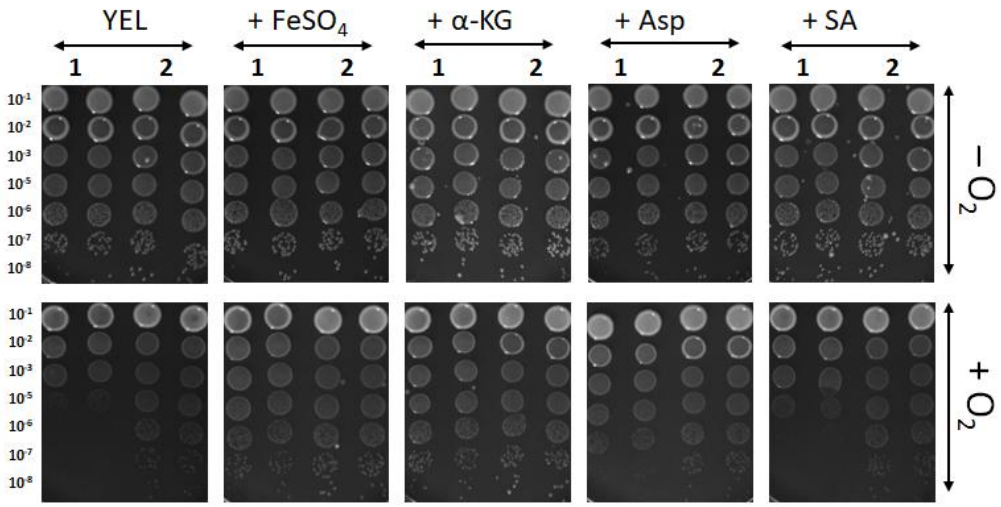

555 **Figure 6.** Colony formation of DSM 4902 (1) and DSM 20271 (2) under anaerobic (-O2) and aerobic (+O2) conditions on
556 YEL agar plates with and without supplementation of FeSO4 (1 mM), aspartic acid (10 mM), α-ketoglutaric acid (1 mM),
557 or succinic acid (1 mM) after four (anaerobic) or six (aerobic) days of incubation at 30°C. The images are representative
558 of experiments repeated at least three times for each condition. YEL, yeast extract – lactate medium; α-KG, α-
559 ketoglutarate; Asp, aspartate; SA, succinate.

560 improved the colony-forming ability of DSM4902, while aspartate and succinate had a lesser effect
561 **(Fig. 6)**. Moreover, DSM 20271 formed small colonies under aerobic conditions even without
562 supplementation. The addition of $FeSO_4$ and α-ketoglutaric acid increased the size of DSM20271
563 colonies under aerobic conditions **(Fig. 6)**. α-ketoglutarate and succinate are important
564 intermediates in the TCA cycle, while aspartic acid can be metabolized in various ways, including
565 conversion to another TCA intermediate, oxaloacetate. Thus, it is tempting to suggest that the
566 addition of these metabolites in YEL enhances the flow of carbon and energy through the TCA cycle,
567 thereby promoting growth and colony-forming ability under aerobic conditions. On the other hand,
568 iron is crucial for various cellular processes, including electron transport in the respiratory chain.
569 Thus, iron sulfate can help improve the efficiency of energy production by supporting the function
570 of iron-containing enzymes in the bacterium's electron transport chain.

571 ***$FeSO_4$ controls the production of heme in the presence of oxygen.*** $FeSO_4$ supplementation was
572 found to enhance the colony formation ability under aerobic conditions, which potentially occurred
573 through increased heme production and the activity of heme-dependent enzymes (e.g.,
574 cytochromes, catalase, peroxides). To study this further, DSM 20271 was cultured in triplicate for
575 96 hours under microaerobic conditions, with and without 1 mM $FeSO_4$, while control cultures were
576 propagated anaerobically.

577 Results revealed no impact on final cell densities with $FeSO_4$ supplementation (data not shown).
578 However, under microaerobic conditions, the addition of $FeSO_4$ elevated heme production and
579 reduced B12 vitamin production **(Fig. 7).** This suggests a shift in tetrapyrrole synthesis toward heme
580 in the presence of excess oxygen and iron, at the expense of B12 production. Superior B12 produc-

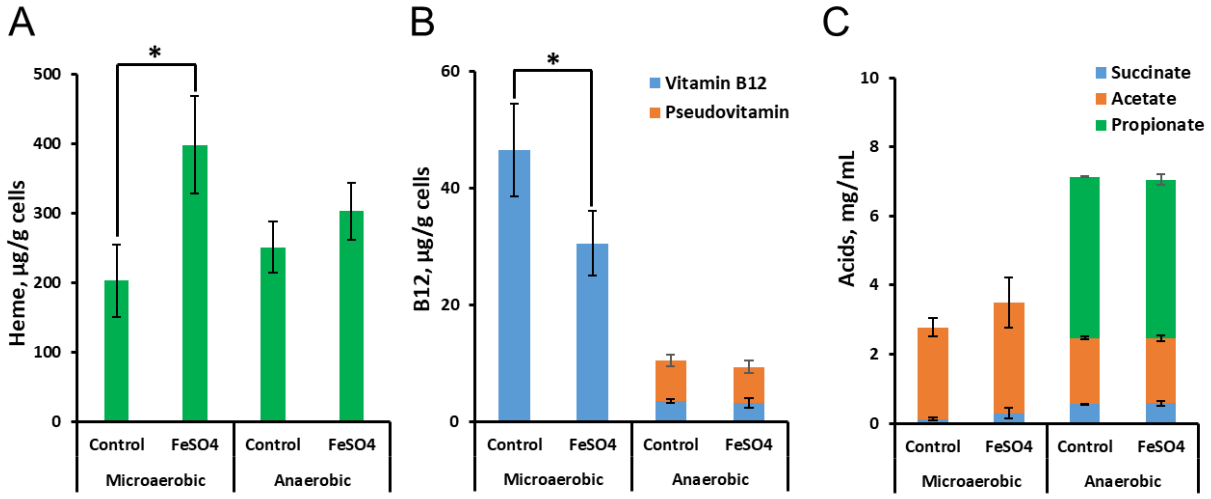

581 **Figure 7.** Effect of $FeSO_4$ (1 mM) supplementation on the biosynthesis of heme **(A)**, vitamin B12 **(B)**, and accumulation
582 of organic acids **(C)** when grown under microaerobic and anaerobic conditions in yeast extract-lactate medium
583 supplemented with $CoCl_2$ (5 mg/L). The values are means and standard deviations of three biological replicates. A
584 significant difference between the treatments ($p < 0.05$) is indicated by an asterisk.

585 tion under microaerobic conditions aligns with a previous report by Dank et al. (17) as well as our
586 bioreactor results **(Fig. S1BF)**. Notably, the cobamide detected under microaerobic conditions is the
587 B12 form, while both pseudo-B12 and B12 forms are produced under anaerobic conditions **(Fig. 7)**.
588 Acetate and succinate were present in all samples, while propionic acid was exclusive to anaerobic
589 conditions, indicating potential differences in propionic acid metabolism under microaerobic
590 conditions (16).

591 **3. Conclusion**

592 We investigated the metabolism and growth characteristics of *PFR* DSM 20271 under aerobic and
593 anaerobic conditions. Our results showed enhanced biomass formation under aerobic conditions.
594 Additionally, lactate consumption was faster under anaerobic conditions, while propionate and
595 acetate levels increased over time under anaerobic conditions but remained low under aerobic
596 conditions. Cobamide synthesis was notably impacted by oxygen, with minimal B12 or pseudo-B12
597 production under aerobic conditions compared to anaerobic or microaerobic conditions. Genes
598 related to iron and α-ketoglutarate transport and metabolism, succinate metabolism, and
599 alanine/aspartate transferase activity were found up-regulated under aerobic conditions, indicating
600 energy production through respiration and classifying PFR as a facultative anaerobe. Surfaceome
601 analyses revealed an oxygen-dependent increase in peptidoglycan hydrolyzing enzymes (RpfA and
602 LytG) along with a several r-proteins and other cytoplasmic proteins. This suggests that PFR may
603 utilize controlled cell lysis or vesiculation to release cytoplasmic moonlighters, influenced by
604 changes in cell surface structures or gene expression triggered by oxygen. Moreover, our study
605 demonstrated that the growth of DSM 20271 under aerobic conditions could be enhanced by
606 supplementation with FeSO4, aspartate, α-ketoglutarate, or succinate. Interestingly, FeSO4
607 supplementation also increased heme production at the expense of B12 production in the presence
608 of oxygen, suggesting a negative effect of externally available iron on B12 synthesis in *PFR*. In
609 summary, our findings underscore the significant role of oxygen in the metabolism and growth of
610 *PFR* DSM 20271, impacting lactate consumption, organic acid production, vitamin synthesis, and
611 cell surface protein abundance.

612

613 # 4. Materials and Methods

614 ## 4.1 Culture conditions

615 Strain DSM 20271 was grown in yeast extract-lactate-based medium (YEL) and routinely cultured at
616 30 °C starting by streaking from glycerol stock (15 %, -80 °C) onto a solid medium (supplemented
617 with 1.5 % agar) and growing for four days in anaerobic jars (Anaerocult, Merck). Liquid cultures
618 were obtained by inoculation of three separated colonies into 10 mL of liquid medium in 15 ml
619 Greiner tubes and propagation for three days at 30 °C without shaking. Experimental cultures were
620 routinely inoculated to 1 % (v/v) and 1.5 % (v/v) in test tubes and bioreactors, respectively. All
621 experiments were performed with three biological replicates.

622

623 ## 4.2 Cell density and viable cell count

624 Cell densities were assessed by measuring the optical density (OD) at a wavelength of 600 nm
625 (OD600) by aseptically removing small aliquotes from the bioreactors. This measurement was
626 routinely taken during the 72-h bioreactor cultivations. Microbial counts were determined using
627 the plate counting technique. Dilution series were prepared in sterile Saline (0.9% NaCl) or PBS, and
628 appropriate dilutions were either spread (100 µL) or spotted (10 µL) onto YEL agar plates. After
629 incubation for 4-7 days in anaerobic conditions using Anaerocult (Merck) at a temperature of 30 °C,
630 colonies were counted, and the CFU/mL (colony-forming units per milliliter) were determined.

631

632 ## 4.3 Fermentation in bioreactors and sampling

633 To investigate the effect of available oxygen on gene expression, growth kinetics, and metabolic
634 activity, batch fermentations were conducted in bioreactors under aerobic and anaerobic
635 conditions.

636 Under aerobic conditions, the pO2 level at 20% was maintained throughout the cultivation process,
637 recognizing the significant impact of increasing cell density and fluid viscosity on oxygen transfer
638 efficiencies - a concern that can be mitigated by controlling oxygen partial pressure (pO2) in
639 bioreactors conducted experiments (73). This decision aimed to ensure optimal oxygen availability,
640 consistent with the reported oxygen conditions in a minimal lactate medium. During anaerobic
641 growth, the pO2 level was verified to be at 0% to ensure the absence of oxygen in the experiment.

642

643 The fermentations were carried out in Sartorius A bioreactors with a growth volume of 750 mL. The
644 temperature was maintained at 30 °C, and the pH was controlled at 7.0 using NaOH (5 M) and HCl

645 (1 M). Stirring was set at 200 rpm for anaerobic experiments. In anaerobic conditions, continuous
646 nitrogen gas flow at 20 cc was utilized, while in aerobic conditions, the oxygen saturation level was
647 maintained at 20% through air and oxygen gas flow, with stirring alternating between 200-300 rpm.

648 Samples of 12 mL were taken aseptically in three biological replicates at four-time points (I-IV) for
649 each atmospheric condition. For anaerobic fermentation, the sampling points were at 12 h (I), 26 h
650 (II), 32 h (III), and 46 h (IV). In aerobic fermentation, samples were collected at 13 h (I), 40 h (II), 52
651 h (III), and 66 h (IV). Surfaceome analyses were performed on samples from the initial time point (I)
652 in both aerobic and anaerobic fermentations. For gene expression and ddPCR analysis, samples
653 from time points I and III were analyzed.

654 Cell harvesting was conducted by centrifugation at 3220 x g for 10 min at +4 °C. The supernatants
655 were collected and stored at -80 °C for acid and vitamin analyses. Harvested cells for vitamin
656 analysis were washed with 1 M Tris-HCl buffer (pH 8.0) and stored at -20 °C.

657 For RNA sequencing, the harvested cells were immediately resuspended in 1500 µL of RNA later
658 (Invitrogen™) and incubated overnight at +4 °C. After incubation, the cells were harvested by
659 centrifugation at 12,000 G for 5 min at +4 °C and stored at -80 °C.

660

661 **4.4 RNA extraction and purification**

662 Cells stored at -80 °C were thawed and resuspended in 50 µL of Tris-EDTA buffer (TE buffer). The
663 cell suspension was then transferred to lysing matrix tubes containing glass beads. Cell lysis was
664 performed using the FastPrep-24 homogenizer, with three cycles of 30 seconds each at a speed of
665 6.5 M/S. Between cycles, the samples were kept on ice for 60 seconds to maintain the temperature.
666 After the final ice incubation, the lysates were suspended in 150 µL of TE buffer and thoroughly
667 vortexed. Subsequently, the lysates were centrifuged at 12,000 g for 5 min at +4 °C to remove cell
668 debris and glass beads. The supernatants were carefully collected and stored at -20 °C.

669 Total RNA extraction was carried out using the RNeasy Mini Kit (Qiagen) according to the
670 manufacturer's instructions, including DNase digestion to remove any remaining DNA. The RNA was
671 eluted with 40 µL of nuclease-free water.

672 Following RNA extraction, the samples underwent DNAase treatment and were further purified
673 using an RNA clean-up method. The concentration of purified single-stranded RNA was measured
674 using a NanoDrop spectrophotometer. The RNA samples were divided into aliquots and stored at -
675 80 °C. To deplete ribosomal RNA (rRNA), the Ribo-Zero Plus rRNA Depletion Kit (Illumina Inc., USA)
676 was employed, following the protocol provided by the manufacturer.

677 **4.5 RNA sequencing and data analysis**

678 The RNA-seq libraries were generated using the QIAseq Stranded Total RNA Lib kit from Qiagen,
679 and sequencing was performed on the Illumina NextSeq 500 platform.

680 To assess the quality of the sequencing reads, FastQC v0.11.7 was employed. Adapter sequences
681 and low-quality reads (using parameters -m 30 -q 25) were removed using cutadapt v1.9.1. Reads
682 that mapped to rRNA sequences were eliminated using sortmerna v2.1, while the remaining reads
683 were aligned to the *PFR* DSM 20271 genome assembly GCF_000940845.1_ASM94084v1 using the
684 mem algorithm of BWA v0.7.11. The number of reads mapped to each gene was counted using
685 Htseq-count v0.1.11. Differential expression analysis was performed using DESeq2 (74), comparing
686 atmospheric conditions (anaerobic versus aerobic) within growth phases (logarithmic and
687 stationary). Additional detailed information on the validation of the RNAseq data with ddPCR is
688 provided in the supplemental material.

689 The RNA-seq data can be accessed at the National Center for Biotechnology Information under the
690 accession PRJNA872337 (https://www.ncbi.nlm.nih.gov/sra/PRJNA872337).

691 Genes were considered to be significantly differentially expressed if their adjusted p-value (padj)
692 was ≤ 0.05 and fold changes were ≥ 2.0 (log2Fold ≥ 1). Predicted GO terms for the genes were
693 obtained using PANNZER2 (75) with default parameters. The lists of differentially expressed genes
694 from the various comparisons were analyzed for enrichment of GO terms in the Biological Process
695 ontology using the R package clusterProfiler (v. 4.0) (76, 77). The reference set used for the analysis
696 included all the genes annotated with GO terms in the genome. The annotated GO terms were
697 visualized using Cytoscape 3.9.1 (78) with the ClueGO plug-in (79).

698

699 **4.6 UHPLC Analysis of Vitamin B12 and Pseudovitamin**

700 Analysis for the active vitamin B12 and pseudovitamin was based on ultra-high performance liquid
701 chromatography (UHPLC) method described by Chamlagain et al. (80). The B12 was extracted in its
702 cyano form from cellular pellets using established methods, as detailed by Chamlagain et al. (80,
703 81). Specifically, 0.1–0.2 g of the cell pellet underwent extraction with a pH 4.5 buffer (comprising
704 8.3 mM sodium hydroxide and 20.7 mM acetic acid) in the presence of sodium cyanide, yielding a
705 25 mL extract. The analysis was performed with Waters UPLCsystem (Waters, Milford, MA, USA)
706 with a C18 column (Waters Acquity HSS T3, 2.1 x 100 mm, 1.8 µm) at a flow rate of 0.32 mL/min, a
707 UV detection by a photodiode array (PDA) detector at 361 nm and an injection volume of 5-15 µL
708 were used. Cyanocobalamin was identified based on retention time and absorption spectrum and
709 quantified against its standard.

710 **4.7 HPLC method to analyze acids and glucose**

711 Glucose, acetic acid (AA), lactic acid (LA), propionic acid (PA), pyruvate and succinate were
712 determined using a high-performance liquid chromatography (HPLC) method described in
713 Chamlagain et al. (81) with modifications. Samples were centrifuged at 12,000 x g for 10 min, and
714 the resulting supernatants were collected. After syringe filtration (Pall, MI, USA; 0.2 µm), the
715 samples were stored at -20 °C. Analyses were conducted on the thawed samples. The analysis was
716 performed on a Hi-Plex H column (Agilent, CA, USA; 300x6.5 mm), with a HiPlex H guard column
717 (Agilent, CA, USA; 50 x 7.7 mm). The HPLC system was equipped with a Waters 515 pump,
718 autosampler, ultraviolet (UV) detector (Waters 717), and refractive index detector (HP 1047A, HP,
719 USA). The mobile phase was 10 mM H_2SO_4, and the flow rate was set at 0.5ml/min for 35 min with
720 the column temperature maintained at 40 °C.

721

722 **4.8 Quantitative heme analysis**

723 The inoculated YEL was incubated at 30 °C under microaerobic and anaerobic conditions for 4 days.
724 To create a microaerobic condition, the cultures (20 mL) were grown in 100-mL glass bottles under
725 shaking conditions (200 rpm) and opened once every day in a sterile environment. The medium was
726 supplemented with 5 mg/L CoCl2 and in the case of Fe-supplemented samples, $FeSO_4$ was also
727 added (1 mM). After incubation, the cultures were centrifuged (6800 × g, 10 min at room
728 temperature). B12 and heme were measured in cells, while the supernatants were analyzed for the
729 organic acid contents.

730 Samples for heme measurements were prepared as follows. A portion of the cell pellet (0.1 g) was
731 suspended in 0.1 mL of 0.1 M NaOH (82) in lysing matrix tubes containing glass beads and the cells
732 were lysed using the FastPrep-24 homogenizer (5 cycles of 30 seconds each at a speed of 4.5 M/s).
733 To maintain the temperature, the samples were kept on ice for 60 seconds between the cycles.
734 Another 0.1 mL of NaOH was added to the cell lysates, homogenized, and centrifuged (12,000 g for
735 10 min at room temperature). The supernatants were carefully collected and analyzed for the heme
736 concentration.

737 Heme concentrations were measured using a heme assay kit (MAK316, Sigma-Aldrich, St. Louis,
738 MO, USA) according to the manufacturer's instructions. Absorbance was measured at 405 nm. The
739 concentration of heme in the samples was calculated against the heme calibrant. The heme content
740 is reported as µg heme/g cells.

741

742 **4.9 Colony forming ability using spot-plating assay**

743 *PFR* DSM 4902 and DSM 20271 cells were grown at 30°C in YEL liquid medium for 3d until OD_{600}
744 reached approximately 1.2. Cells were pelleted by centrifugation, washed once with PBS, and
745 resuspended in PBS to the same OD_{600}, serially 10-fold diluted, and spotted (5 µl of dilutions) on YEL
746 agar plates supplemented with appropriate chemicals. Plates were incubated under anaerobic or
747 aerobic conditions at 30°C for 4 days (anaerobic) or 6 days (aerobic).

748

749 **4.10 Surfaceome analyses**

750 ***Preparing the cell samples for proteomics and enzymatic cell-surface shaving.*** The surfaceome
751 samples were harvested from mid-log (I) growth phases of both aerobic and anaerobic
752 fermentations by centrifugation (4 min, 4 °C, 3320× g). The cells were washed with 0.1 M sodium
753 acetate (pH 5.0, Sigma-Aldrich) and resuspended into 50 mM TEAB (17% sucrose)
754 (triethylammonium bicarbonate buffer, Sigma-Aldrich) after centrifugation (4 min, 4 °C, 3320× g).
755 Enzymatic surface shaving was carried out with 0.05 µg/µL of trypsin (Promega, Madison, WI, USA)
756 for 30 min at 37 °C. Afterward, the protein-cell suspensions were first time centrifuged (4 min, RT,
757 4000× g) to ensure cell-free supernatant and second time centrifuged (2 min, RT, 16 000× g) through
758 Spin-X® filters to recover the peptides and the enzyme. Flow-troughs were left to incubate for 17 h
759 at 37 °C before the tryptic digestions were terminated with the addition of trifluoroacetic acid (TFA,
760 Sigma-Aldrich) at a final concentration of 0.6%. The peptide concentrations were measured
761 spectrophotometrically with NanoDrop- 1000 (Thermo Fisher Scientific, DE, USA). Samples were
762 stored at - 20 °C.

763 ***LC-MS/MS identification.*** The tryptic peptides were concentrated and purified using ZipTips C_{18}
764 (Merck Millipore) according to the manufacturer's instructions. An equal amount of each peptide
765 sample was loaded into an Easy-nLC 1000 nano-LC system (Thermo Scientific, Waltham, MA, USA)
766 coupled with a quadrupole Orbitrap mass spectrometer (Q ExactiveTM, ThermoElectron, Bremen,
767 Germany) equipped with a nano-electrospray ion source (EASY- SprayTM, Thermo Scientific,
768 Waltham, MA, USA), and analyzed as previously described (83). The acquired MS raw files, for
769 protein identification and label-free quantification (LFQ), were searched against an in-house
770 database of DSM 20271T (CP010341) (18) with MaxQuant (ver. 1.6.1.0) under the following
771 settings: carbamidomethyl (C) was specified as a fixed modification; oxidation of methionine was
772 set as a variable modification; a peptide tolerance was set at 20 ppm in the first search and the main
773 search error of 4.5 ppm was applied. Additionally, trypsin without proline restriction enzyme option

774 was used, allowing two miscleavages; the false discovery rate (FDR) filtering was set to 1 % for both
775 peptide and protein identification, and the minimal number of unique and razor peptides were
776 defined as 1.

777 ***Surfaceome bioinformatics and statistics.*** The identified proteins were submitted to SignalP 5.0
778 (84), SecretomeP 2.0 (85), LipoP 1.0 (86, 87) and TatP 1.0 (88) analysis tools to determine the
779 presence of possible classical and non-classical signal peptide sequences. Additionally, the
780 prediction of protein transmembrane helices was acquired by TMHMM Server v. 2.0 (89, 90),
781 general protein function annotation, according to the COG, was accomplished with EggNOG 5.0.0
782 (91) and the isoelectric points (pIs) and molecular weights (MWs) were predicted by EMBOSS
783 Pepsats (92).

784 The statistical comparisons of the MaxQuant-derived protein identifications were performed in
785 Perseus version 1.6.15.0 (93), at which the known contaminant, reverse hits, and proteins only
786 identified by site were excluded. The MS-raw intensities were filtered to contain minimally 2/3 valid
787 values in at least one of the growth environments to obtain the total and unique identifications.
788 Statistical comparisons of the normalized log2-transformed LFQ levels were also carried out in
789 Perseus. The data were filtered to include proteins with valid LFQ-values in at least 70% of biological
790 replicates in at least one group. Before a Student's t-test with a permutation-based false discovery
791 rate of 0.05, the missing values were imputed from a normal distribution using parameters: width
792 0.3 and downshift 1.8. A complete linkage hierarchical clustering was performed on normalized (Z-
793 score) values. The mass spectrometry proteomics data have been deposited to the
794 ProteomeXchange Consortium via the PRIDE (94) partner repository with the dataset identifier
795 PXD051703.

796

797 **Data availability statement**

798 The transcriptomics and proteomics data sets generated during and/or analysed during the current
799 study are available in the SRA database under the accession PRJNA872337 and PRIDE repository
800 with dataset identifiers PXD051703. The other data sets generated during and/or analysed during
801 the current study and not included in the manuscript are available from the corresponding author
802 on reasonable request.

803

804

Acknowledgements

Funding for this study was provided by the University of Helsinki Doctoral School in Environmental, Food and Biological Sciences. The study was also funded by Academy of Finland (project number 325784), Novo Nordisk Foundation (project number NNF20OC0065096), core Facilities programme of the South-Eastern Norway Regional Health Authority (TN), Research Council of Norway INFRASTRUKTUR-programme (295910). We also thank Finnish Food and Drink Industries' Federation (ETL) for their support in funding the research.

The following core facilities are acknowledged for their services and support, which were essential for this work: Institute of Biotechnology, DNA Sequencing and Genomics, University of Helsinki, Proteomics Core Facility at Oslo University Hospital.

Author contributions

IL: Study design and experimental work – transcriptomics, acids, vitamin, cell counts, Writing – original draft

AS: Study design and experimental work – proteomics, Writing – original draft

PD: Experimental work – Bioinformatics, Writing – review

BC: Methodology – Acid, vitamin & heme, Supplementation experiment, Writing – original draft

ME: Methodology – Acid and vitamin

PA: Writing – review

TN: Methodology – proteomics, Writing – review, Funding acquisition

KS: Methodology – proteomics, Writing - review & editing

VP: Writing – review

PV: Conceptualization, Supervision, Methodology, Writing – original draft, review & editing, Funding acquisition

Conflict of interest statement

The corresponding authors confirm on behalf of all authors that there have been no involvements that might raise the question of bias in the work reported or in the conclusions, implications or opinions stated.

References

1. Thierry A, Deutsch SM, Falentin H, Dalmasso M, Cousin FJ, Jan G. 2011. New insights into physiology and metabolism of *Propionibacterium freudenreichii*. Int J Food Microbiol 149:19-27.
2. Dank A, Abee T, Smid EJ. 2023. Expanded metabolic diversity of *Propionibacterium freudenreichii* potentiates novel applications in food biotechnology. Curr Opin Food Sci 52:101048.
3. Thierry A, Maillard M-B, Richoux R, Lortal S. 2005. *Propionibacterium freudenreichii* strains quantitatively affect production of volatile compounds in Swiss cheese. Lait 85:57-74.
4. Le Maréchal C, Peton V, Plé C, Vroland C, Jardin J, Briard-Bion V, Durant G, Chuat V, Loux V, Foligné B, Deutsch SM, Falentin H, Jan G. 2015. Surface proteins of *Propionibacterium freudenreichii* are involved in its anti-inflammatory properties. J Proteomics 113:447-61.
5. Rodovalho VdR, Luz BSRd, Rabah H, Do Carmo FLR, Folador EL, Nicolas A, Jardin J, Briard-Bion V, Blottière H, Lapaque N. 2020. Extracellular vesicles produced by the probiotic *Propionibacterium freudenreichii* CIRM-BIA 129 mitigate inflammation by modulating the NF-κB pathway. Front Microbiol 11:1544.
6. Wolffenbuttel BHR, Wouters H, Heiner-Fokkema MR, van der Klauw MM. 2019. The Many Faces of Cobalamin (Vitamin B(12)) Deficiency. Mayo Clin Proc Innov Qual Outcomes 3:200-214.
7. Obeid R, Heil SG, Verhoeven MMA, van den Heuvel EGHM, de Groot LCPGM, Eussen SJPM. 2019. Vitamin B12 Intake From Animal Foods, Biomarkers, and Health Aspects. Front Nutr 6.
8. Assis DAd, Matte C, Aschidamini B, Rodrigues E, Záchia Ayub MA. 2020. Biosynthesis of vitamin B12 by *Propionibacterium freudenreichii* subsp. *shermanii* ATCC 13673 using liquid acid protein residue of soybean as culture medium. Biotechnol Prog 36:e3011.
9. Calvillo Á, Pellicer T, Carnicer M, Planas A. 2023. Developing a single-stage continuous process strategy for vitamin B12 production with *Propionibacterium freudenreichii*. Microb Cell Fact 22:26.
10. Chamlagain B, Edelmann M, Katina K, Varmanen P, Piironen V. 2024. Vitamin B12 production in solubilized protein extract of bioprocessed wheat bran with *Propionibacterium freudenreichii*. LWT - Food Sci Technol 192:115731.
11. Roessner CA, Huang K-x, Warren MJ, Raux E, Scott AI. 2002. Isolation and characterization of 14 additional genes specifying the anaerobic biosynthesis of cobalamin (vitamin B12) in *Propionibacterium freudenreichii* (*P. shermanii*). Microbiol 148:1845-1853.
12. Deptula P, Kylli P, Chamlagain B, Holm L, Kostiainen R, Piironen V, Savijoki K, Varmanen P. 2015. BluB/CobT2 fusion enzyme activity reveals mechanisms responsible for production of active form of vitamin B_{12} by *Propionibacterium freudenreichii*. Microb Cell Fact 14:186.
13. Kruk M, Varmanen P, Edelmann M, Chamlagain B, Trząskowska M. 2024. Food by-product valorisation in nutrients through spent brewer's yeast bioprocessing with *Propionibacterium freudenreichii*. J Clean Prod 434:140102.
14. Piwowarek K, Lipińska E, Hać-Szymańczuk E, Kolotylo V, Kieliszek M. 2022. Use of apple pomace, glycerine, and potato wastewater for the production of propionic acid and vitamin B12. App Microbiol Biotechnol 106:5433-5448.
15. Xie C, Coda R, Chamlagain B, Edelmann M, Varmanen P, Piironen V, Katina K. 2021. Fermentation of cereal, pseudo-cereal and legume materials with *Propionibacterium freudenreichii* and *Levilactobacillus brevis* for vitamin B12 fortification. LWT 137:110431.
16. Dank A, van Mastrigt O, Boeren S, Lillevang SK, Abee T, Smid EJ. 2021. *Propionibacterium freudenreichii* thrives in microaerobic conditions by complete oxidation of lactate to CO(2). Environ Microbiol 23:3116-3129.
17. Dank A, Biel G, Abee T, Smid EJ. 2022. Microaerobic metabolism of lactate and propionate enhances vitamin B(12) production in *Propionibacterium freudenreichii*. Microb Cell Fact 21:225.
18. Koskinen P, Deptula P, Smolander OP, Tamene F, Kammonen J, Savijoki K, Paulin L, Piironen V, Auvinen P, Varmanen P. 2015. Complete genome sequence of *Propionibacterium freudenreichii* DSM 20271(T). Stand Genomic Sci 10:83.
19. Falentin H, Deutsch SM, Jan G, Loux V, Thierry A, Parayre S, Maillard MB, Dherbécourt J, Cousin FJ, Jardin J, Siguier P, Couloux A, Barbe V, Vacherie B, Wincker P, Gibrat JF, Gaillardin C, Lortal S. 2010. The complete genome of *Propionibacterium freudenreichii* CIRM-BIA1, a hardy actinobacterium with food and probiotic applications. PLoS One 5:e11748.

887 20. Deptula P, Laine PK, Roberts RJ, Smolander O-P, Vihinen H, Piironen V, Paulin L, Jokitalo E, Savijoki
888 K, Auvinen P. 2017. De novo assembly of genomes from long sequence reads reveals uncharted
889 territories of *Propionibacterium freudenreichii*. BMC Genom 18:1-24.
890 21. Pizarro F, Olivares M, Hertrampf E, Mazariegos DI, Arredondo M. 2003. Heme-iron absorption is
891 saturable by heme-iron dose in women. J Nutr 133:2214-7.
892 22. Zhang J, Cui Z, Zhu Y, Zhu Z, Qi Q, Wang Q. 2022. Recent advances in microbial production of high-
893 value compounds in the tetrapyrrole biosynthesis pathway. Biotechnol Adv 55:107904.
894 23. Crow VL. 1986. Utilization of Lactate Isomers by *Propionibacterium freudenreichii* subsp. *shermanii*:
895 Regulatory Role for Intracellular Pyruvate. Appl Environ Microbiol 52:352-8.
896 24. Hartman T, Weinrick B, Vilchèze C, Berney M, Tufariello J, Cook GM, Jacobs Jr WR. 2014. Succinate
897 dehydrogenase is the regulator of respiration in *Mycobacterium tuberculosis*. PLoS pathogens
898 10:e1004510.
899 25. Pinchuk GE, Rodionov DA, Yang C, Li X, Osterman AL, Dervyn E, Geydebrekht OV, Reed SB, Romine
900 MF, Collart FR. 2009. Genomic reconstruction of *Shewanella oneidensis* MR-1 metabolism reveals a
901 previously uncharacterized machinery for lactate utilization. Proc Natl Acad Sci U S A 106:2874-
902 2879.
903 26. Brzuszkiewicz E, Weiner J, Wollherr A, Thürmer A, Hüpeden J, Lomholt HB, Kilian M, Gottschalk G,
904 Daniel R, Mollenkopf HJ, Meyer TF, Brüggemann H. 2011. Comparative genomics and
905 transcriptomics of *Propionibacterium acnes*. PLoS One 6:e21581.
906 27. Leaver FW, Wood HG, Stjernholm R. 1955. The fermentation of three carbon substrates by
907 Clostridium propionicum and Propionibacterium. J Bacteriol 70:521-30.
908 28. Parizzi LP, Grassi MC, Llerena LA, Carazzolle MF, Queiroz VL, Lunardi I, Zeidler AF, Teixeira PJ,
909 Mieczkowski P, Rincones J, Pereira GA. 2012. The genome sequence of *Propionibacterium*
910 *acidipropionici* provides insights into its biotechnological and industrial potential. BMC Genomics
911 13:562.
912 29. Banerjee R, Gouda H, Pillay S. 2021. Redox-Linked Coordination Chemistry Directs Vitamin B(12)
913 Trafficking. Acc Chem Res 54:2003-2013.
914 30. Deptula P. 2017. A multifaceted study of *Propionibacterium freudenreichii*, the food-grade
915 producer of active vitamin B12. PhD thesis. University of Helsinki, Finland.
916 31. Li J, Ge Y, Zadeh M, Curtiss III R, Mohamadzadeh M. 2020. Regulating vitamin B12 biosynthesis via
917 the cbiM Cbl riboswitch in *Propionibacterium* strain UF1. Proc Natl Acad Sci U S A 117:602-609.
918 32. Vitreschak AG, Rodionov DA, Mironov AA, Gelfand MS. 2003. Regulation of the vitamin B12
919 metabolism and transport in bacteria by a conserved RNA structural element. RNA 9:1084-1097.
920 33. Mellin JR, Koutero M, Dar D, Nahori M-A, Sorek R, Cossart P. 2014. Sequestration of a two-
921 component response regulator by a riboswitch-regulated noncoding RNA. Science 345:940-943.
922 34. Polaski JT, Holmstrom ED, Nesbitt DJ, Batey RT. 2016. Mechanistic insights into cofactor-dependent
923 coupling of RNA folding and mRNA transcription/translation by a cobalamin riboswitch. Cell Rep
924 15:1100-1110.
925 35. Fang H, Kang J, Zhang D. 2017. Microbial production of vitamin B 12: a review and future
926 perspectives. Microb cell fact 16:1-14.
927 36. Martens J-H, Barg H, Warren Ma, Jahn D. 2002. Microbial production of vitamin B 12. Appl
928 Microbiol Biotechnol 58:275-285.
929 37. Piao Y, Kiatpapan P, Yamashita M, Murooka Y. 2004. Effects of Expression of *hemA* and *hemB*
930 Genes on Production of Porphyrin in *Propionibacterium freudenreichii*. Appl Environ 70:7561-7566.
931 38. Outten FW, Wood MJ, Munoz FM, Storz G. 2003. The SufE protein and the SufBCD complex
932 enhance SufS cysteine desulfurase activity as part of a sulfur transfer pathway for Fe-S cluster
933 assembly in *Escherichia coli*. J Biol Chem 278:45713-45719.
934 39. Blahut M, Sanchez E, Fisher CE, Outten FW. 2020. Fe-S cluster biogenesis by the bacterial Suf
935 pathway. Biochim Biophys Acta 1867:118829.
936 40. Huet G, Daffé M, Saves I. 2005. Identification of the *Mycobacterium tuberculosis* SUF machinery as
937 the exclusive mycobacterial system of [Fe-S] cluster assembly: evidence for its implication in the
938 pathogen's survival. J Bacteriol 187:6137-6146.

939 41. Frohnmeyer E, Deptula P, Nyman TA, Laine PKS, Vihinen H, Paulin L, Auvinen P, Jokitalo E, Piironen
940 V, Varmanen P, Savijoki K. 2018. Secretome profiling of *Propionibacterium freudenreichii* reveals
941 highly variable responses even among the closely related strains. Microb Biotechnol 11:510-526.
942 42. Griffin ME, Klupt S, Espinosa J, Hang HC. 2023. Peptidoglycan NlpC/P60 peptidases in bacterial
943 physiology and host interactions. Cell Chem Biol 30:436-456.
944 43. Amblee V, Jeffery CJ. 2015. Physical Features of Intracellular Proteins that Moonlight on the Cell
945 Surface. PLoS One 10:e0130575.
946 44. Granato D, Bergonzelli GE, Pridmore RD, Marvin L, Rouvet M, Corthésy-Theulaz IE. 2004. Cell
947 surface-associated elongation factor Tu mediates the attachment of *Lactobacillus johnsonii*
948 NCC533 (La1) to human intestinal cells and mucins. Infect Immun 72:2160-9.
949 45. N'Diaye AR, Borrel V, Racine PJ, Clamens T, Depayras S, Maillot O, Schaack B, Chevalier S,
950 Lesouhaitier O, Feuilloley MGJ. 2019. Mechanism of action of the moonlighting protein EfTu as a
951 Substance P sensor in *Bacillus cereus*. Sci Rep 9:1304.
952 46. Henderson B, Fares MA, Lund PA. 2013. Chaperonin 60: a paradoxical, evolutionarily conserved
953 protein family with multiple moonlighting functions. Biol Rev Camb Philos Soc 88:955-87.
954 47. An M, Lim Y-H. 2023. Surface-exposed chaperonin 60 derived from *Propionibacterium*
955 *freudenreichii* MJ2 inhibits adipogenesis by decreasing the expression of C/EBPα/PPARγ. Sci Rep
956 13:19251.
957 48. González-López MA, Velázquez-Guadarrama N, Romero-Espejel ME, Olivares-Trejo Jde J. 2013.
958 *Helicobacter pylori* secretes the chaperonin GroEL (HSP60), which binds iron. FEBS Lett 587:1823-8.
959 49. Kana BD, Gordhan BG, Downing KJ, Sung N, Vostroktunova G, Machowski EE, Tsenova L, Young M,
960 Kaprelyants A, Kaplan G, Mizrahi V. 2008. The resuscitation-promoting factors of *Mycobacterium*
961 *tuberculosis* are required for virulence and resuscitation from dormancy but are collectively
962 dispensable for growth in vitro. Mol Microbiol 67:672-84.
963 50. Wang W, Jeffery CJ. 2016. An analysis of surface proteomics results reveals novel candidates for
964 intracellular/surface moonlighting proteins in bacteria. Mol Biosyst 12:1420-31.
965 51. Berlec A, Zadravec P, Jevnikar Z, Štrukelj B. 2011. Identification of candidate carrier proteins for
966 surface display on *Lactococcus lactis* by theoretical and experimental analyses of the surface
967 proteome. Appl Environ Microbiol 77:1292-300.
968 52. Celebioglu HU, Svensson B. 2017. Exo- and surface proteomes of the probiotic bacterium
969 *Lactobacillus acidophilus* NCFM. Proteomics 17.
970 53. Koskenniemi K, Laakso K, Koponen J, Kankainen M, Greco D, Auvinen P, Savijoki K, Nyman TA,
971 Surakka A, Salusjärvi T, de Vos WM, Tynkkynen S, Kalkkinen N, Varmanen P. 2011. Proteomics and
972 transcriptomics characterization of bile stress response in probiotic *Lactobacillus rhamnosus* GG.
973 Mol Cell Proteomics 10:M110.002741.
974 54. Tjalsma H, Lambooy L, Hermans PW, Swinkels DW. 2008. Shedding & shaving: disclosure of
975 proteomic expressions on a bacterial face. Proteomics 8:1415-28.
976 55. Rodovalho VdR, da Luz BSR, Nicolas A, Do Carmo FLR, Jardin J, Briard-Bion V, Jan G, Le Loir Y, de
977 Carvalho Azevedo VA, Guédon E. 2021. Environmental conditions modulate the protein content
978 and immunomodulatory activity of extracellular vesicles produced by the probiotic
979 *Propionibacterium freudenreichii*. Appl Environ Microbiol 87:e02263-20.
980 56. Rodovalho VdR, da Luz BSR, Nicolas A, Jardin J, Briard-Bion V, Folador EL, Santos AR, Jan G, Loir YL,
981 Azevedo VAdC. 2023. Different culture media and purification methods unveil the core proteome
982 of *Propionibacterium freudenreichii*-derived extracellular vesicles. Microlife 4:uqad029.
983 57. Pang Y, Ermann Lundberg L, Mata Forsberg M, Ahl D, Bysell H, Pallin A, Sverremark-Ekstroem E,
984 Karlsson R, Jonsson H, Roos S. 2022. Extracellular membrane vesicles from *Limosilactobacillus*
985 *reuteri* strengthen the intestinal epithelial integrity, modulate cytokine responses and antagonize
986 activation of TRPV1. Front Microbiol 13:1032202.
987 58. Codemo M, Muschiol S, Iovino F, Nannapaneni P, Plant L, Wai SN, Henriques-Normark B. 2018.
988 Immunomodulatory effects of pneumococcal extracellular vesicles on cellular and humoral host
989 defenses. mBio 9:10.1128/mbio. 00559-18.
990 59. Lee EY, Choi DY, Kim DK, Kim JW, Park JO, Kim S, Kim SH, Desiderio DM, Kim YK, Kim KP. 2009.
991 Gram-positive bacteria produce membrane vesicles: proteomics-based characterization of
992 *Staphylococcus aureus*-derived membrane vesicles. Proteomics 9:5425-5436.

60. Rivera J, Cordero RJ, Nakouzi AS, Frases S, Nicola A, Casadevall A. 2010. *Bacillus anthracis* produces membrane-derived vesicles containing biologically active toxins. Proc Natl Acad Sci U S A 107:19002-19007.
61. Ebner P, Götz F. 2019. Bacterial excretion of cytoplasmic proteins (ECP): occurrence, mechanism, and function. Trends Microbiol 27:176-187.
62. Ebner P, Luqman A, Reichert S, Hauf K, Popella P, Forchhammer K, Otto M, Götz F. 2017. Non-classical protein excretion is boosted by PSMα-induced cell leakage. Cell Reports 20:1278-1286.
63. Ebner P, Prax M, Nega M, Koch I, Dube L, Yu W, Rinker J, Popella P, Flötenmeyer M, Götz F. 2015. Excretion of cytoplasmic proteins (ECP) in *Staphylococcus aureus*. Mol Microbiol 97:775-789.
64. Ebner P, Rinker J, Götz F. 2016. Excretion of cytoplasmic proteins in *Staphylococcus* is most likely not due to cell lysis. Curr Genet 62:19-23.
65. Götz F, Yu W, Dube L, Prax M, Ebner P. 2015. Excretion of cytosolic proteins (ECP) in bacteria. IJMM 305:230-237.
66. Pagani TD, Guimaraes ACR, Waghabi MC, Correa PR, Kalume DE, Berredo-Pinho M, Degrave WM, Mendonca-Lima L. 2019. Exploring the potential role of moonlighting function of the surface-associated proteins from *Mycobacterium bovis* BCG Moreau and Pasteur by comparative proteomic. Front Immunol 10:716.
67. Savijoki K, Myllymäki H, Luukinen H, Paulamäki L, Vanha-Aho L-M, Svorjova A, Miettinen I, Fallarero A, Ihalainen TO, Yli-Kauhaluoma J. 2021. Surface-shaving proteomics of *Mycobacterium marinum* identifies biofilm subtype-specific changes affecting virulence, tolerance, and persistence. mSystems 6:10.1128/msystems. 00500-21.
68. Krasowska A, Sigler K. 2014. How microorganisms use hydrophobicity and what does this mean for human needs? Front Cell Infect Microbiol 4:112.
69. Castro FD, Sedman J, Ismail AA, Asadishad B, Tufenkji N. 2010. Effect of dissolved oxygen on two bacterial pathogens examined using ATR-FTIR spectroscopy, microelectrophoresis, and potentiometric titration. Environ Sci Technol 44:4136-4141.
70. Wang J, Karki C, Xiao Y, Li L. 2020. Electrostatics of prokaryotic ribosome and its biological implication. Biophysical Journal 118:1205-1212.
71. de Vries W, Wijck-Kapteijn WM, Stouthamer AH. 1972. Influence of oxygen on growth, cytochrome synthesis and fermentation pattern in propionic acid bacteria. J Gen Microbiol 71:515-24.
72. Ye K, Shijo M, Jin S, Shimizu K. 1996. Efficient production of vitamin B12 from propionic acid bacteria under periodic variation of dissolved oxygen concentration. J Ferm Bioeng 82:484-491.
73. Garcia-Ochoa F, Gomez E. 2009. Bioreactor scale-up and oxygen transfer rate in microbial processes: an overview. Biotechnol Adv 27:153-176.
74. Love MI, Huber W, Anders S. 2014. Moderated estimation of fold change and dispersion for RNA-seq data with DESeq2. Genome Biol 15:550.
75. Törönen P, Holm L. 2022. PANNZER-A practical tool for protein function prediction. Protein Sci 31:118-128.
76. Wu T, Hu E, Xu S, Chen M, Guo P, Dai Z, Feng T, Zhou L, Tang W, Zhan L, Fu X, Liu S, Bo X, Yu G. 2021. clusterProfiler 4.0: A universal enrichment tool for interpreting omics data. The Innovation 2:100141.
77. Yu G, Wang LG, Han Y, He QY. 2012. clusterProfiler: an R package for comparing biological themes among gene clusters. Omics 16:284-7.
78. Shannon P, Markiel A, Ozier O, Baliga NS, Wang JT, Ramage D, Amin N, Schwikowski B, Ideker T. 2003. Cytoscape: a software environment for integrated models of biomolecular interaction networks. Genome Res 13:2498-504.
79. Bindea G, Mlecnik B, Hackl H, Charoentong P, Tosolini M, Kirilovsky A, Fridman WH, Pagès F, Trajanoski Z, Galon J. 2009. ClueGO: a Cytoscape plug-in to decipher functionally grouped gene ontology and pathway annotation networks. Bioinformatics 25:1091-3.
80. Chamlagain B, Edelmann M, Kariluoto S, Ollilainen V, Piironen V. 2015. Ultra-high performance liquid chromatographic and mass spectrometric analysis of active vitamin B12 in cells of *Propionibacterium* and fermented cereal matrices. Food Chem 166:630-638.

1045 81. Chamlagain B, Deptula P, Edelmann M, Kariluoto S, Grattepanche F, Lacroix C, Varmanen P,
1046 Piironen V. 2016. Effect of the lower ligand precursors on vitamin B12 production by food-grade
1047 Propionibacteria. LWT - Food Sci Technol 72:117-124.
1048 82. Yang S, Wang A, Li J, Shao Y, Sun F, Li S, Cao K, Liu H, Xiong P, Gao Z. 2023. Improved biosynthesis
1049 of heme in *Bacillus subtilis* through metabolic engineering assisted fed-batch fermentation. Microb
1050 Cell Fact 22:102.
1051 83. Savijoki K, Miettinen I, Nyman TA, Kortesoja M, Hanski L, Varmanen P, Fallarero A. 2020. Growth
1052 Mode and Physiological State of Cells Prior to Biofilm Formation Affect Immune Evasion and
1053 Persistence of *Staphylococcus aureus*. Microorganisms 8.
1054 84. Almagro Armenteros JJ, Tsirigos KD, Sønderby CK, Petersen TN, Winther O, Brunak S, von Heijne G,
1055 Nielsen H. 2019. SignalP 5.0 improves signal peptide predictions using deep neural networks. Nat
1056 Biotechnol 37:420-423.
1057 85. Bendtsen JD, Kiemer L, Fausbøll A, Brunak S. 2005. Non-classical protein secretion in bacteria. BMC
1058 Microbiol 5:58.
1059 86. Juncker AS, Willenbrock H, Von Heijne G, Brunak S, Nielsen H, Krogh A. 2003. Prediction of
1060 lipoprotein signal peptides in Gram-negative bacteria. Protein Sci 12:1652-62.
1061 87. Rahman O, Cummings S, Harrington D, Sutcliffe I. 2008. Methods for the bioinformatic
1062 identification of bacterial lipoproteins encoded in the genomes of Gram-positive bacteria. World J
1063 Microbiol Biotechnol 24:2377-2382.
1064 88. Bendtsen JD, Nielsen H, Widdick D, Palmer T, Brunak S. 2005. Prediction of twin-arginine signal
1065 peptides. BMC Bioinformatics 6:167.
1066 89. Krogh A, Larsson B, von Heijne G, Sonnhammer EL. 2001. Predicting transmembrane protein
1067 topology with a hidden Markov model: application to complete genomes. J Mol Biol 305:567-80.
1068 90. Sonnhammer EL, von Heijne G, Krogh A. 1998. A hidden Markov model for predicting
1069 transmembrane helices in protein sequences. Proc Int Conf Intell Syst Mol Biol 6:175-82.
1070 91. Huerta-Cepas J, Szklarczyk D, Heller D, Hernández-Plaza A, Forslund SK, Cook H, Mende DR, Letunic
1071 I, Rattei T, Jensen LJ, von Mering C, Bork P. 2019. eggNOG 5.0: a hierarchical, functionally and
1072 phylogenetically annotated orthology resource based on 5090 organisms and 2502 viruses. Nucleic
1073 Acids Res 47:D309-d314.
1074 92. Rice P, Longden I, Bleasby A. 2000. EMBOSS: the European Molecular Biology Open Software Suite.
1075 Trends Genet 16:276-7.
1076 93. Tyanova S, Temu T, Sinitcyn P, Carlson A, Hein MY, Geiger T, Mann M, Cox J. 2016. The Perseus
1077 computational platform for comprehensive analysis of (prote)omics data. Nat Methods 13:731-40.
1078 94. Perez-Riverol Y, Bai J, Bandla C, García-Seisdedos D, Hewapathirana S, Kamatchinathan S, Kundu
1079 DJ, Prakash A, Frericks-Zipper A, Eisenacher M. 2022. The PRIDE database resources in 2022: a hub
1080 for mass spectrometry-based proteomics evidences. Nucleic Acids Res 50:D543-D552.

1081

1082

1083

1084

1085

1086

1087

1088

1089 **Supplementary Materials**

1090 **Table S1.** Results of RNA sequencing of the strain *P. freudenreichii* DSM 20271 grown in bioreactors
1091 under anaerobic (nitrogen) and aerobic (oxygen) atmospheres at sampling points I and III. Columns
1092 A-I specify the order of annotated genes, locus tags of the current NCBI annotations, the previous
1093 version of the NCBI locus tags, product names, locations in the genome and strand orientation.
1094 Column J-AM: results of DEseq2 analyses with models comparing the effect of atmosphere
1095 (anaerobic vs. aerobic) at both sampling points (columns J-O); the effect of atmosphere (aerobic vs.
1096 anaerobic) at sampling point I (columns P-U); the effect of atmosphere (aerobic vs. anaerobic) at
1097 sampling point III (columns V-AA); the effect of growth phase under anaerobic atmosphere
1098 (columns AB-AG) and the effect of growth phase under aerobic atmosphere (AH-AM). Columns AN-
1099 BA list results from previously reported bioinformatics analyses (Deptula et al**.,** 2017), including
1100 annotations with PROKKA, core genes identified through comparative analyses against other *PFR*
1101 strains with ROARY, IslandViewer, Prophinder, Phaster, REBASE and CRISPRFinder.

1102

1103 **Table S2.** List of 74 genes encoding transport proteins detected with more than two-fold higher
1104 expression under anaerobic conditions.

1105

1106 **Table S3.** List of all identified proteins with the detected raw intensity values for each. Reverse hits,
1107 potential contaminants, and proteins only identified by site were filtered out. Proteins were filtered
1108 to contain minimally 2/3 valid values in at least one of the growth environments. The number of
1109 transmembrane spanning domains (TMD) were predicted using TMHMM 2.0, subcellular
1110 localization of proteins were done with prediction tool PSORTb 3.0.3, and the presence of possible
1111 classical and non-classical signal peptide sequences were analysed with LipoP 1.0, SignalP 5.0, and
1112 SecretomeP 2.0. The COG categorization was accomplished with EggNOG 5.0.0.

1113

1114 **Table S4.** Proteins uniquely identified in at least two out of three replica samples in aerobic or
1115 anaerobic growth conditions. The colour gradient from pink to red indicates the log-2 transformed
1116 raw intensities for each biological replicate (grey colour indicates zero). The number of
1117 transmembrane spanning domains (TMD) were predicted using TMHMM 2.0, subcellular
1118 localization of proteins were done with prediction tool PSORTb 3.0.3 PSORTb v3.0.2, and the
1119 presence of possible classical and non-classical signal peptide sequences were analysed with LipoP
1120 1.0, SignalP 5.0, and SecretomeP 2.0. The COG categorization was accomplished with EggNOG 5.0.0.

1121

1122 **Table_S5.** List of proteins showing statistically significant protein abundance change between the
1123 aerobic and anaerobic surfaceomes. For this purpose, the LFQ intensities after log2 conversion and
1124 missing value imputation were subjected to two-sample t-test with a permutation-based false
1125 discovery rate of 0.05 to confirm the statistical significance. The number of transmembrane
1126 spanning domains (TMD) were predicted using TMHMM 2.0, subcellular localization of proteins
1127 were done with prediction tool PSORTb 3.0.3 PSORTb v3.0.2, and the presence of possible classical
1128 and non-classical signal peptide sequences were analysed with LipoP 1.0, SignalP 5.0, and
1129 SecretomeP 2.0. The COG categorization was accomplished with EggNOG 5.0.0.
1130
1131 **Figure_S1.** (A) Cell densities (OD600 values - solid line) and cell viability (CFU/mL - dotted line) in
1132 bioreactors conducted experimented under aerobic (green) and microaerobic (blue) growth
1133 conditions. (B) Lactate utilization (A), excreted propionate (B), acetate (C), pyruvate (D), succinate
1134 (E) and intracellular vitamin B12 of P. freudenreichii DSM 20271 during cultivation under aerobic
1135 (green) and microaerobic (blue) fermentations performed in bioreactors. n = 3. In aerobic
1136 fermentation, samples were collected at 13 h (I), 40 h (II), 52 h (III), and 66 h (IV). For microaerobic
1137 fermentation, samples were obtained at 12 h (I), 26 h (II), 22 h (III), and 51 h (IV).
1138
1139 **Supplemental material.** Material, methods and results for validation of RNAseq data with ddPCR.